



1 **A Multi-site Passive Approach for Studying the Emissions and**  
2 **Evolution of Smoke from Prescribed Fires**

3 Rime El Asmar<sup>1</sup>, Zongrun Li<sup>2</sup>, David J. Tanner<sup>1</sup>, Yongtao Hu<sup>2</sup>, Susan O'Neill<sup>3</sup>, L. Gregory Huey<sup>1</sup>,  
4 M. Talat Odman<sup>2</sup>, Rodney J. Weber<sup>1</sup>

5 <sup>1</sup>School of Earth and Atmospheric Sciences, Georgia Institute of Technology, Atlanta, 30331, USA.

6 <sup>2</sup>School of Civil and Environmental Engineering, Georgia Institute of Technology, Atlanta, 30331, USA.

7 <sup>3</sup>USDA Forest Service, Pacific Northwest Research Station, 400 North 34th Street, Suite 201, Seattle, WA 98103,  
8 USA.

9

10 *Correspondence to:* Rodney J. Weber ([rweber@eas.gatech.edu](mailto:rweber@eas.gatech.edu))

11



12 **Abstract.** We conducted a two-year study utilizing a network of fixed sites with sampling throughout an extended  
13 prescribed burning period to characterize the emissions and evolution of smoke from silvicultural prescribed burning  
14 in the southeastern US. The measurement approach and an assessment of instrument performance is described. Smoke  
15 sources are identified, and plume ages are determined to quantify emissions and study the evolution of smoke  $PM_{2.5}$   
16 mass, black carbon (BC), and brown carbon (BrC). Over the 2021 and 2022 prescribed burning seasons (nominally  
17 January to May,) we identified 64 smoke events based on high levels of  $PM_{2.5}$  mass, BC, BrC, and carbon monoxide  
18 (CO), of which 61 were linked to a specific burning area. Smoke transport times were estimated using the mean wind  
19 speed along with distance between fire and measurement site, and with HYSPLIT back trajectories.  $PM_{2.5}$  emission  
20 ratios based on  $\Delta PM_{2.5} \text{ mass} / \Delta CO$  for fresh smoke (age  $\leq 1$  hour) ranged between 0.04 and  $0.18 \mu\text{g m}^{-3} \text{ppb}^{-1}$  with a  
21 mean of  $0.117 \mu\text{g m}^{-3} \text{ppb}^{-1}$  (median of  $0.121 \mu\text{g m}^{-3} \text{ppb}^{-1}$ ). Both the mean emission ratio and variability were similar  
22 to findings from other prescribed fire studies, but lower than wildfires. Mean emission ratios of BC and BrC were  
23  $0.014 \mu\text{g m}^{-3} \text{ppb}^{-1}$  and  $0.442 \text{Mm}^{-1} \text{ppb}^{-1}$  respectively. Ozone enhancements ( $\Delta O_3$ ) were always observed in plumes  
24 detected in the afternoon.  $\Delta PM_{2.5} \text{ mass} / \Delta CO$  was observed to increase with plume age in all ozone enhanced plumes  
25 suggesting photochemical secondary aerosol formation. In contrast,  $\Delta BrC / \Delta CO$  was not found to vary with plume  
26 ages less than 8 hours during photochemically active periods.



## 27 1. Introduction

28 Large and intense wildfires have been increasing over the past few decades in the US and their emissions are  
29 a critical concern (Singleton et al., 2019; Jaffe et al., 2020). Fire is also an essential ecological process and prescribed  
30 burning, which is the act of starting controlled fires for specific purposes, is an important tool for restoration of  
31 ecosystems, land management, and reducing fuel to prevent destructive wildfires (Kelp et al., 2023). Prescribed fires  
32 are typically conducted during favorable conditions associated with the fuel type and amount, soil moisture, and  
33 meteorology. In 2018, the USDA Forest Service indicated a high risk of hazardous wildfires over approximately 234  
34 million acres of forest lands in the US (Wyden and Manchin, 2020). However, federal land management authorities  
35 were able to conduct prescribed fires on only approximately 4.6 million acres in 2018, and averaged about 4.1 million  
36 acres per year between 2009-2018 (Wise, 2022). The southeastern US has a long history of using prescribed fires, for  
37 example roughly 2.18, 1.26, and 0.94 million acres were burned in 2017 in Florida, Georgia, and Alabama  
38 respectively, representing almost two thirds of the prescribed burning conducted nationally (as published by Statista  
39 Research Department based on National Interagency Coordination Center in March 20, 2018). The National  
40 Interagency Coordination Center estimated that the total prescribed fire acres burned in 2017 nationally was 6.43  
41 million acres. Recognizing the need to mitigate the size and severity of wildfires, prescribed burning is anticipated to  
42 increase in the coming years (USDA, 2022).

43 While prescribed burning can be performed under favorable weather conditions, it can still contribute to  
44 serious local and regional air pollution as it is a source of primary and secondary air pollutants (Lee et al., 2008). Like  
45 other types of biomass burning, prescribed burning releases high amounts of particulate matter, CO, and inorganic  
46 and organic compounds (Lee et al., 2005), which have negative effects on health and visibility (Bell, 2004; Huang et  
47 al., 2019). Prescribed fires are often conducted at urban-rural interfaces creating a buffer zone to prevent the spread  
48 of wildfires towards the built environment. However, this means that the planned fires often occur closer to populated  
49 areas, and potentially lead to high population exposure due to this proximity. Although prescribed fires generally  
50 produce less pollutants by consuming less fuel per area burned than wildfires, the population health costs can be  
51 substantially higher for prescribed fires due to burning near higher population densities (Borchers-Arriagada et al.,  
52 2021).

53 Both wildfires and prescribed fires emit a large variety of gases and particulates (Liu et al., 2017b; Burling  
54 et al., 2011). Gases include nitrogen oxides and volatile organic compounds that can form ozone and secondary  
55 particulate matter. Hazardous air pollutants are also produced but they may be less detrimental to exposed populations  
56 than particulates (O'Dell et al., 2022). PM<sub>2.5</sub>, (particulate matter with aerodynamic diameter of 2.5 micrometers or  
57 smaller), is directly emitted as primary particles and also formed from condensation of emitted gases and their  
58 oxidation products, where a major component is secondary organic aerosol (SOA) (Liu et al., 2016; May et al., 2014).  
59 PM<sub>2.5</sub> exposure has been linked in many epidemiological studies to serious health problems such as respiratory,  
60 cardiovascular, and neurological diseases, as well as increased risk of adverse birth outcomes (Liu et al., 2015; Reid  
61 et al., 2016; Naeher et al., 2007). Given their significant impact on the environment and health, satellite, airborne, or  
62 ground-based studies of smoke emissions have been extensively conducted.



63            Detection and characterization of wildland fires is an important step towards assessing their impacts. Remote  
64 sensing via satellites can detect wildland fires by thermal anomalies (Kuenzer et al., 2008) or vegetation changes  
65 (Mildrexler et al., 2007). Satellite-based approaches are highly useful (Ichoku and Kaufman, 2005; Christopher et al.,  
66 1998; Kaufman et al., 1989; Martinsson et al., 2022), but there are limitations, including temporal coverage and spatial  
67 resolution (both horizontal and vertical) (Liu et al., 2019; Ichoku et al., 2016), detector sensitivity, interferences (e.g.,  
68 clouds or surface conditions), and interactions between different emissions (Liu et al., 2019; Wang et al., 2018; Martin  
69 et al., 2018). This can lead to significant under-detection of fires and limitations in quantifying emissions needed to  
70 determine population exposures, especially for lower intensity prescribed fires (Nowell et al., 2018; Larkin et al.,  
71 2020; Martin et al., 2018; Buysse et al., 2019; Jaffe et al., 2020).

72            Aircraft (fixed wing and helicopters) and more recently drones are commonly used in airborne studies of  
73 wildland fires (Decker et al., 2021b; Cubison et al., 2011) and have been deployed for prescribed burning studies  
74 (Yokelson et al., 1999; May et al., 2014; Pratt et al., 2011). Airborne studies provide high spatial resolution data,  
75 however, it is non-continuous, and can miss certain aspects of smoke emissions, such as longer-term smoldering,  
76 especially at night (Burling et al., 2011). Employing a combination of airborne and ground-based measurements can  
77 be beneficial in providing a comprehensive view of the plume (Burling et al., 2011; Akagi et al., 2014; Yokelson et  
78 al., 2013; Strand et al., 2016).

79            In ground-based studies, measurement sites can be mobile or fixed. Mobile labs may capture dynamic air  
80 quality patterns and to some extent assess spatial distributions in plumes (Levy et al., 2014). However, they are usually  
81 limited in space and instrumentation capacity. Interferences from the power source, vibration and speed changes  
82 during transportation can affect instrument stability and performance leading to inaccurate measurements or limiting  
83 the type of instruments that can be used. Attempting to track wildland smoke plumes can be challenging due to  
84 unpredictable winds and dispersion conditions combined with access limitations. For example, Burling et al. reports  
85 successfully sampling smoke from 2 out of 14 prescribed fires using a battery powered mobile FTIR system (Burling  
86 et al., 2011).

87            Fixed monitoring stations equipped with various instruments provide continuous, localized measurements  
88 for short or long-term monitoring for studies assessing diurnal, seasonal, and long-term trends in air pollution. Multiple  
89 sites provide spatial coverage within a region. A variety of highly sensitive instruments can be deployed, ensuring  
90 accurate and precise measurements of various pollutants that can be compared with air quality data across different  
91 locations for regional assessments (Strand et al., 2016).

92            The overall goal of this study was to investigate the emissions and evolution of prescribed fires and to provide  
93 data to test model simulations. Results from a two-year study utilizing fixed monitoring stations and continuous  
94 sampling in a region of active prescribed burning are presented. The observations are analyzed to determine emission  
95 ratios of PM<sub>2.5</sub> mass, BC, and BrC and their variability. Not all smoke from the prescribed fires in the region is detected  
96 so the overall impact of all fires on regional air quality cannot be determined and is better addressed by a model  
97 simulation. Instead, our goal is to sample multiple smoke events so that an analysis of the data will provide a robust  
98 characterization of smoke from prescribed burning in the region and sufficient data to test model simulations. In the



99 following sections, we describe the methodology, data analysis approach, case studies on various detected or missed  
100 smoke plumes, and initial findings on emission estimates of PM<sub>2.5</sub> mass, BC, and BrC and their evolution. These  
101 findings are needed to assess the impact of prescribed burns on a variety of public health and policy issues.

## 102 **2. Method**

### 103 **2.1. Site description**

104 Prescribed burning at Fort Moore Army Base, (formerly Fort Benning), in west central Georgia, United  
105 States, was studied during March through May of 2021 and February through May of 2022. Since 1981, prescribed  
106 burning has been used as a land management tool at the 182,000 acres military base, of which 145,000 acres are  
107 forested lands. Vegetation is characterized by pine-dominated uplands, and hardwood-dominated bottomlands.  
108 Unintended small wildfires ignited during military training exercises also occur at the base and the land managers  
109 have been recording data on both prescribed fires and wildfires since the 1980s. Prescribed burning at the Fort has  
110 been effective; it has reduced the frequency of wildfires from ~ 300-500 wildfires/year in the early 1980s to less than  
111 100 wildfires/year in the mid-1990s. During this period the prescribed fire burnt area changed from ~7,500 acres in  
112 1981 to ~ 12,000 acres in 1992. Currently, 30,000 woodland acres are burned annually using controlled fires, with a  
113 future planned burning of 45,000 acres annually. Prescribed burning occurs from December through May when there  
114 is sufficient but not excessive rainfall, and suitable temperatures and wind conditions to burn deadwood, brush, and  
115 low-growing vegetation accumulating on the forest floor. The area of the base is divided into 332 burn units that range  
116 in size from 100 to 1,800 acres and are burnt alternately every two to three years.

### 117 **2.2. Measuring sites**

118 One instrumented research trailer (7'W x 18'L x 6.5'H) was deployed in the 2021 burning season (March 18,  
119 2021 to May 15, 2021), and successively trailers (6'W x 12'L x 7'H) were added in 2022 (February 11, 2022 to May  
120 18, 2022) reaching a total of five trailers located at different sites throughout the Fort. In 2021, the one trailer operated  
121 at the same location until it was moved on April 26, 2021 to a new site for the remaining season as expected burning  
122 regions at the Fort changed. The trailers sampled continuously, except during periods of power loss or technical issues.  
123 The locations of trailers, shown in Fig. 1, were chosen based on power availability, prevailing wind, and burning plans  
124 set prior to the burning season.

### 125 **2.3. Instrumentation**

126 To characterize the prescribed fire smoke, the trailers were equipped with several instruments selected based  
127 on factors such as availability, ability for extended stand-alone operation, and their significance to the study. All  
128 sampling was done through inlets nominally 4 m above ground level and 1.5 m above the trailer roof.

129 Measurements included, carbon monoxide (CO), nitrogen oxides (NO, NO<sub>2</sub>, NO<sub>x</sub>), ozone (O<sub>3</sub>), PM<sub>2.5</sub> mass  
130 concentration and black carbon (BC) concentration and brown carbon (BrC) light absorption coefficients. Carbon  
131 monoxide is a long-lived species, with a typical lifetime of ~ 1 month, emitted during incomplete combustion and  
132 used as a smoke tracer to track its movement and dispersion (Forrister et al., 2015; Liu et al., 2016). Other forms of  
133 incomplete combustion emissions (e.g., mobile sources) and oxidation of VOCs are also CO sources. CO mixing ratios



134 were measured by IR analyzers (Thermo Fisher Scientific Inc, model 48C, Franklin, MA) with a lower detection limit  
135 (LOD) of 0.04 ppm at an averaging time of 390 seconds. The measurements alternated between blank and ambient  
136 measurements every 195 seconds. The blanks were determined with a custom-built CO scrubber made of 0.5 % Pd on  
137 alumina catalyst heated to 180 °C (Parrish et al., 1994), which oxidizes CO to CO<sub>2</sub>. Calibration of CO analyzers was  
138 performed before and after each field study using a 100 ppm CO in air standard purchased from nexAir (Memphis,  
139 TN).

140 O<sub>3</sub> was measured using an ultraviolet (UV) photometric analyzer (Thermo Fisher Scientific Inc, model 49C,  
141 Franklin, MA) zeroed through an O<sub>3</sub> scrubber in the instrument, with LOD of 1.0 ppb and averaging time of 20  
142 seconds. The analyzer was calibrated before and after each field deployment using an O<sub>3</sub> calibrator (Thermo Fisher  
143 Scientific Inc, model 49C, Franklin, MA). NO<sub>x</sub> species were measured using a chemiluminescence NO-NO<sub>2</sub>-NO<sub>x</sub>  
144 analyzer (Thermo Fisher Scientific Inc, model 42i, Franklin, MA). The NO<sub>x</sub> analyzer was calibrated automatically  
145 every 6 hours, using NO and NO<sub>2</sub> calibration standards purchased from Airgas (Radnor, PA) and has an LOD of 0.40  
146 ppb.

147 PM<sub>2.5</sub> mass concentration was determined with a Tapered Element Oscillating Microbalance (TEOM) series  
148 1400a ambient particulate monitor (Thermo Fisher Scientific, Franklin, MA) with data recorded at an averaging time  
149 of 60 seconds and typical detection limit of 5.58 µg m<sup>-3</sup> determined by 3 standard deviations of blank (filtered ambient  
150 air) measurements. This data was subsequently averaged to time intervals of 20 and 60 minutes to mitigate noise,  
151 especially when sampling under background conditions. The TEOM is a US-EPA approved instrument for measuring  
152 the mass concentration of ambient PM<sub>2.5</sub> and PM<sub>10</sub> (Liu et al., 2017a). It is a gravimetric measurement that determines  
153 the mass accumulated on a microbalance over a specified time interval at a monitored sample air flow rate. The sample  
154 air is preconditioned to a temperature of 50 °C to remove liquid water interferences. Mass concentration over an  
155 averaging period is calculated from the difference recorded between successive intervals. Due to random fluctuations  
156 in the instrument operation when concentrations are low, this can lead to negative numbers, illustrated by the frequency  
157 distribution of high time resolution data recorded by one TEOM shown in Fig. S1. When determining the average  
158 background concentration, we include the negative mass concentrations since converting negative concentrations to  
159 one half the LOD or ignoring them will produce an average that is biased high. In 2021, PM<sub>10</sub> TEOMs were also  
160 deployed but this was found to be highly influenced by pollen, which can be high in the springtime, and so the  
161 measurement was discontinued. Regional hourly PM<sub>2.5</sub> mass was reported at two Environmental Protection Division  
162 (EPD) sites. In the following analysis we compare the PM<sub>2.5</sub> measured within the Fort to the EPD measurements at  
163 the Columbus Airport and Phenix City South Girard (PCSG) school shown on the map in Fig. 1a.

164 PM<sub>2.5</sub> black carbon (BC) mass concentration was measured by aethalometers. A range of multi and single  
165 wavelength instruments were deployed. Two were seven wavelength instruments (Magee Scientific, model AE33 and  
166 model AE31, Berkeley, CA) with detection ranges of 0.1–100 µg m<sup>-3</sup> and averaging times of 60 and 120 seconds  
167 respectively, one 2-wavelength aethalometer (Magee Scientific, model AE22, Berkeley, CA) of 0.1 µg m<sup>-3</sup> detection  
168 limit and 60 seconds averaging time, and two single wavelength particle soot absorption photometers (PSAPs)  
169 (Radiance Research, Seattle, WA) of sensitivity > 0.1 µg m<sup>-3</sup> for 60 seconds averaging time. For the multiwavelength



170 aethalometers, BC was determined from the light absorption at 880 nm using the manufacturer's specified mass  
171 absorption cross-section (MAC) of  $7.77 \text{ m}^2 \text{ g}^{-1}$ , whereas for the single wavelength PSAPs, BC was determined from  
172 the optical absorption coefficient at 565 nm assuming a specific mass absorption cross-section of  $10 \text{ m}^2 \text{ g}^{-1}$  following  
173 the manufacturer's specifications. Two spot samplings of the model AE33 corrected for mass loading errors. This was  
174 not done in the other instruments and so the data of the aethalometers (AE31 and AE22) were corrected for loading  
175 interference using the method of Virkkula et al. (Virkkula et al., 2007). PSAPs measurements were not corrected due  
176 to unavailability of scattering coefficients needed for correcting filter-based PSAP measurements (Bond et al., 1999;  
177 Virkkula et al., 2005), which may lead to 10-20% underestimation of BC at sites where PSAPs were installed.

178 Brown carbon (BrC) was calculated from the 7-wavelength aethalometer measurements. BrC is largely  
179 produced from biomass burning (Hecobian et al., 2010) and in the following analysis used as a unique indicator of  
180 biomass burning smoke. While a small amount of BrC can be produced from mobile sources and other sources of  
181 incomplete combustion, in the US, its predominant source is biomass burning (Jo et al., 2016; Hecobian et al., 2010).  
182 We calculate the light absorption of BrC at 365 nm as a marker for BrC levels. Using the aethalometer data, the  
183 absorption coefficient, which corresponds to (BC+BrC), was inferred by multiplying mass concentration at each  
184 wavelength by the corresponding MAC value provided by the manufacturer (Magee Scientific, Berkeley, CA).  
185 The absorption coefficient at 365 nm was determined by extrapolating the linear regression of log absorption  
186 coefficient vs log wavelength since the lowest wavelength at which the aethalometer operates is 370 nm. The slope of  
187 the linear relationship represents the negative of the absorption Angstrom Exponent (AAE), a parameter used to study  
188 the optical properties of the aerosol. BrC at 365 nm was then calculated by removing the estimated contribution of BC  
189 at 365 nm assuming that BrC does not absorb at 880 nm and that AAE of pure BC is 1. BrC absorption at shorter  
190 wavelengths is the difference of aethalometer-measured total absorption and the extrapolated BC absorption (Lack  
191 and Langridge, 2013). All data of the light absorption of BrC discussed in this work corresponds to the absorption  
192 calculated at 365 nm. Both  $\text{AAE}_{\text{total}}$  and  $\text{AAE}_{\text{BrC}}$  were calculated as the negative slopes of log absorption coefficient  
193 of total (BC+BrC) and BrC respectively, as a function of log wavelengths. For  $\text{AAE}_{\text{total}}$  the fit included wavelengths  
194 370–880 nm (i.e., 370, 470, 520, 590, 660, 880), whereas for  $\text{AAE}_{\text{BrC}}$  the wavelengths ranged from 370 to 660nm (i.e.,  
195 370, 470, 520, 590, 660).

196 We used meteorological data from the Remote Automated Weather Stations (RAWS) located at the base in  
197 our analysis, shown in Fig. 1a. In each trailer, all instruments were connected to a laptop computer with remote access  
198 to reduce personnel time spent at the sites. Sites were generally visited every 1 to 2 weeks during which regular  
199 instrument checks and maintenance was performed, such as restoring power, changing filters (for TEOMs and PSAPs),  
200 measuring and recording flow rates and other instrument performance parameters.

#### 201 **2.4. Tools and analysis methods**

202 *Normalized Excess Mixing Ratios:* To account for dilution of species of interest in a smoke plume,  
203 Normalized Excess Mixing Ratios (NEMRs) are used. The NEMR is the ratio of enhancement of a studied species  
204 above the local background concentrations to the enhancement of a long-lived component co-emitted from the biomass  
205 burning event. CO is often used as the reference species, i.e., NEMR of species X is  $\Delta X/\Delta Y$ , where Y is CO measured



206 in the same sample as X. To determine the NEMR of X and the contribution of smoke to X from an identified burning  
207 region, the background concentration of X (i.e., concentration if no smoke emissions) is subtracted from the  
208 measurement. In our study we used the average of the measurements before and after the smoke event as the  
209 background since sampling was not performed upwind of the fire. This method is supported by the observation from  
210 multiple sampling sites of spatially uniform background concentrations and, in most cases, very low background  
211 concentrations relative to those recorded in the smoke. However, there is more uncertainty when calculating  $O_3$   
212 NEMRs due to significant levels and diurnal changes in background concentrations. NEMRs can also be determined  
213 from the slope of linear regressions. Here, we determine NEMRs in each smoke event for  $PM_{2.5}$  mass, BC, and BrC  
214 normalized by CO by first removing background concentrations for data recorded during the event and then calculating  
215 the slope by linear regressions (i.e., the slope of  $PM_{2.5}$  mass concentration, BC concentration, or BrC absorption at  
216 365 nm versus CO concentrations to determine the respective NEMRs).

217 *Determining Smoke Sources and Plume Age:* To match specific fires to observed smoke at the monitoring  
218 sites, several methods were used. Data from the Fire Information for Resource Management System (FIRMS)  
219 provided active fire data based on thermal anomalies. These are based on measurements from the Moderate Resolution  
220 Imaging Spectroradiometer (MODIS), carried by Aqua and Terra satellites, and the Visible Infrared Imaging  
221 Radiometer Suite (VIIRS), carried by the Suomi National Polar-orbiting Partnership (Suomi NPP) and NOAA-20  
222 satellites. FIRMS provides live and historical fire maps and data that can be accessed online  
223 (<https://firms.modaps.eosdis.nasa.gov/>). This platform can be used to pinpoint specific locations and obtain distances  
224 between points, which is useful for identifying possible fires where smoke was transported to the sampling site and  
225 the time for smoke transport when combined with wind speed and direction data. Although the FIRMS fire map is  
226 updated every 5 minutes, the polar orbiting satellites pass over the location only twice per day meaning that some fires  
227 starting and ending between satellite observations are not detected (Schroeder and Giglio, 2018; Giglio et al., 2021).  
228 Also, small or relatively cool fires may not be detected, especially when there is significant cloud coverage or thick  
229 smoke. Burn data provided by Fort Moore were used with the FIRMS data to minimize limitations with each method  
230 for identifying sources of observed smoke.

231 The Hybrid Single-Particle Lagrangian Integrated Trajectory (HYSPLIT) model (Stein et al., 2015) was used  
232 to calculate back trajectories from monitoring sites. This trajectory analysis was based on meteorological data derived  
233 from the Weather Research and Forecasting (WRF) model (Shamarock et al., 2019) enhanced with grid nudging and  
234 observational nudging (Deng et al., 2009; Liu et al., 2005), using a 20-minute timestep. The WRF domain settings are  
235 shown in Fig. S2. The winds used in the trajectory analysis are from the 1-km grid resolution domain. Each analysis  
236 covered a total of 10 trajectories, all below the planetary boundary layer (PBL). HYSPLIT was run with 10-minute  
237 timesteps, and the locations of fires were determined based on FIRMS data and the Fort Moore Fire Management  
238 records.

### 239 3. Results and discussion

#### 240 3.1. Assessment of $PM_{2.5}$ monitors and background concentrations

241 The focus of this analysis is on  $PM_{2.5}$  mass concentrations from the prescribed fires. Aerosol particle mass  
242 concentrations measurements are difficult, especially at background conditions when concentrations are low.





243 Calibrating instruments with known mass standards is also problematic. We performed intercomparisons between  
244 monitors including direct comparisons for two pairs (side-by-side) and intercomparison of background  $\text{PM}_{2.5}$  mass  
245 concentrations measured by the study TEOMs to the values reported at state monitoring sites. For example, two  
246 TEOMs (used in main and T1293 trailers) collocated at Eglin Air Force Base in 2023 from March 19, 2023 at 8:00  
247 till March 20, 2023 at 10:00, had an orthogonal regression slope of  $0.98 \pm 0.09$ , intercept of  $0.45 \pm 0.37 \mu\text{g m}^{-3}$  and  $r^2$   
248 of 0.84 (see Fig. S3). The main trailer TEOM was also compared with the TEOM used on T1291 when they were  
249 collocated at the Georgia Institute of Technology from September 22, 2023 at 19:00 till October 07, 2023 at 14:00.  
250 Although measurement during that period was close to background levels, the comparison resulted in an orthogonal  
251 regression slope of  $0.88 \pm 0.03$ , intercept of  $3.75 \pm 0.09 \mu\text{g m}^{-3}$  and an  $r^2$  of 0.76 (see Fig. S4). The frequency  
252 distribution used to determine the mean values, and mean background values of the data recorded at the main trailer  
253 and the EPD sites in 2022 are shown in Fig. S5. The mean concentrations in 2022 were 7.02, 9.47, 9.01, 9.26, and  
254  $7.11 \mu\text{g m}^{-3}$  at the main trailer, T1293, T1292, T1921, and T1290 respectively and 10.33 and  $10.67 \mu\text{g m}^{-3}$  at the  
255 Columbus Airport and PCSG school EPD sites respectively. Background air  $\text{PM}_{2.5}$  mass concentrations were also  
256 determined by excluding smoke events (discussed below). The monthly backgrounds of  $\text{PM}_{2.5}$  mass concentrations  
257 are shown in Table S1. Background concentrations were in the range of approximately  $3\text{--}7 \mu\text{g m}^{-3}$  for monitors at the  
258 Fort, and between 7 and  $9 \mu\text{g m}^{-3}$  at the state monitoring sites (Table S2). Higher background  $\text{PM}_{2.5}$  mass  
259 concentrations at the state sites are likely due to the local anthropogenic (urban) influence. These comparisons provide  
260 confidence in the mass measurements that cannot be calibrated in a manner similar to gas monitors.

261 Background concentrations of CO and BC are also given in Table S1. Background CO ranged between  $\sim 150$   
262 and 200 ppb and background BC ranged between 0.14 and  $0.57 \mu\text{g m}^{-3}$ . In terms of spatial variation within Fort Moore,  
263 background levels of measured species were slightly lower in sites located far from the main roads and training areas,  
264 such as measurements at the main trailer during May of 2021 and the entire 2022 season. No significant temporal  
265 variation is observed, although fires within and in the vicinity of the base increase during the transition from winter to  
266 spring, indicating that smoke was efficiently dispersed on time scales of approximately one day. Frequent smoke  
267 events where concentrations of the various measured species were substantially above these background levels were  
268 observed during the 2021 and 2022 field deployments.

### 269 3.2. Study of fires at Fort Moore during 2021 and 2022

270 We first present an overview of the measurements at Fort Moore during two burning seasons. In the 2021  
271 season, only one research (main) trailer was deployed. In the following year, four more were deployed for a total of  
272 five sites.

273 On March 18, 2021, a fully equipped trailer was deployed in the North boundary of Fort Moore, and we  
274 sampled at that location until April 26, 2021. It was then moved to the center of the Fort for sampling from April 26  
275 to May 15, 2021 (see Fig. 1a). During this period, peaks of measured species were observed, as shown in the time  
276 series of  $\text{PM}_{2.5}$  mass in Fig. 2b. Maximum  $\text{PM}_{2.5}$  mass concentrations reached  $2000 \mu\text{g m}^{-3}$  for 20-minute averaged  
277 data and  $1400 \mu\text{g m}^{-3}$  for hourly-averaged data (Table S3). A total of 11  $\text{PM}_{2.5}$  peaks with mass concentrations greater  
278 than  $35 \mu\text{g m}^{-3}$  were recorded. In 2022, over the course of the entire burning season, a total of 53  $\text{PM}_{2.5}$  mass  
279 concentration peaks greater than  $35 \mu\text{g m}^{-3}$  were detected across the five measuring sites, as shown in Fig. 2c with



280 similar high concentrations, reaching  $841 \mu\text{g m}^{-3}$  for 20-minute averaged and  $513 \mu\text{g m}^{-3}$  for hourly-averaged data  
281 (Tables S4 to S7).

282 We focus on the larger smoke plumes to identify their sources and estimate the emissions and evolution of  
283  $\text{PM}_{2.5}$  mass because the burning areas are readily identified (e.g., detected remotely by satellite) and the plume can be  
284 easily delineated from the background. An increase in measured species is considered a peak, or event, when the 20-  
285 minute average  $\text{PM}_{2.5}$  mass is greater than  $35 \mu\text{g m}^{-3}$  and the 40-minute average  $\text{PM}_{2.5}$  mass concentration (average of  
286 two consecutive measurements) is larger than  $30 \mu\text{g m}^{-3}$ . This excludes shorter transient events that includes a passing  
287 vehicle that can occur at measuring sites near training areas.

288 The large peaks in  $\text{PM}_{2.5}$  mass are always accompanied by an increase in CO, BC, and BrC. Figure 3 shows  
289 the scatter plots of 20-minute averaged data collected in 2021 and 2022. The linear relation between  $\text{PM}_{2.5}$  and CO,  
290 BC, and BrC during events resulted in an  $r^2$  of 0.85, 0.68, and 0.71 respectively. These correlations suggest that the  
291 events identified correspond to periods of measuring smoke from biomass burning sources. However, it is important  
292 to note that variability still exists in slopes among different events, which will be explored and discussed in later  
293 sections.

### 294 3.3. Determining smoke sources

295 When a smoke plume is identified the goal is to link it to a specific burn area and determine the transport  
296 time. Identifying the location of prescribed fires was complicated by several factors. In this study, we had limited  
297 beforehand information on the timing and location of planned burns. Moreover, smoke from other sources, such as  
298 prescribed and wildfires in the region, but not within the Fort, as well as uncertainty and variability in wind patterns  
299 at the time of burning, led us to utilize multiple methods to determine the source of each identified smoke episode.

300 Our analysis started by using satellite data from FIRMS to identify locations of fires (when the satellite passed  
301 overhead). After the end of the study, those locations were verified by cross-referencing with the fire management  
302 reports, which provided locations and acreage of prescribed burns and ongoing wildfires exclusively within the Fort  
303 for each day. Afterwards, we pinpointed the source of smoke that reached the monitors by averaging the wind vectors  
304 at and before the peaks using the meteorological data from RAWS. This provided the expected general upwind region  
305 the smoke likely came from. We also used the HYSPLIT model to conduct back trajectory analysis from the  
306 measurement trailer for 8 hours prior to ascertain if the air mass containing the measured smoke had passed the  
307 satellite-identified hot spot or the units reported as burnt by the Fort's Fire Management. HYSPLIT initial altitudes  
308 were determined by the PBL height, where trajectories for 10 equally distributed altitudes between 10 m above the  
309 surface and the top of the PBL were generated for each simulation. For example, if the PBL height was 100 m,  
310 trajectories were calculated at 10, 20, 30, 40, 50, 60, 70, 80, 90, and 100 m.

311 Through the systematic combination of these methods, we attempted to identify specific fire sources  
312 associated with each observed smoke event and the time of transport of the smoke from the fire to the measurement  
313 site (referred to as smoke age). This procedure was successful for 61 out of 64 of the identified smoke events. We  
314 failed to identify 3 events that had no apparent source in agreement with the studied wind patterns. Moreover, of the  
315 61 identified smoke events, 7 events were matched to different sources using the observed wind vector method versus



316 using the HYSPLIT trajectories, 7 events were matched to sources using HYSPLIT only, and 5 events were matched  
317 to sources using wind vector method only.

318 The variability of smoke sources determined in some cases is attributed to the difference between wind  
319 direction used by HYSPLIT and that recorded by RAWS used for the wind vector calculation. In HYSPLIT, wind  
320 data are derived from the three-dimensional wind fields predicted by the application of the WRF model. Figure 4  
321 shows a comparison between modeled and observed wind direction during the events identified in 2021 and 2022 at  
322 the main trailer. A closer alignment in wind direction is observed during higher-speed wind conditions.

323 As an example of source determination, Figure 5a shows the time series of CO, PM<sub>2.5</sub> mass, BC, and BrC  
324 during three smoke episodes recorded on April 6, 7, and 8, 2021, which are indicated by blue, yellow, and green  
325 shading, respectively. Along the top of the graph are the hourly averaged wind vectors based on data from RAWS.  
326 Note the high correlation between PM<sub>2.5</sub> mass and CO concentration and BrC absorption coefficient indicating that  
327 the PM<sub>2.5</sub> peaks were due to smoke. During those three days, the three events were measured during late evening,  
328 nighttime, and early morning periods. In each case, there is a time delay between when the burning occurred and when  
329 the plume was measured, due to the transport time. In all three cases, burning regions at the Fort were identified as  
330 the source. Consider the first smoke event detected at the trailer between 1:00 and 11:00 on April 6, 2021 (blue shaded  
331 region in Fig. 5a). Figure 5b shows the map of the Fort and FIRMS satellite data on the day before (April 5, 2021)  
332 indicating 2 hot spots on the base, which were later verified in the fire report as burning of 2 units and 4 sections of a  
333 third unit. Both burns were to the south and south-southeast of the trailer, and the winds were from the northwest,  
334 west, and southwest during the daytime on April 5, 2021. By midnight, the wind direction shifted, with air flowing  
335 from the south and the southeast, transporting smoke to the trailer's location, leading to elevated concentrations of  
336 species on monitors. Wind speeds were very low at night. At about 8:00, wind speed increased, its direction changed,  
337 and concentrations of the species all dropped.

338 Burning of other units took place on April 6, 2021 at distances 0.8, 2.1, 2.5, 6.3, and 7.2 miles from the trailer.  
339 The level of measured smoke products started increasing in the evening after the winds became southwesterly and  
340 stayed high until the morning of the next day (April 7, 2021) (yellow shaded region in Fig. 5a). Later at night of April  
341 7 (green shaded region in Fig. 5a), concentration levels increased slightly after the burning of two connected units to  
342 the south of the base during the daytime of April 7, 2021 at a distance ranging between 10.8 and 12.5 miles as indicated  
343 by the Fort's Fire Management and seen on FIRMS. HYSPLIT back trajectory analysis, shown in Fig. 5 (e, f, and g),  
344 was conducted for assessing our conclusion on the sources, especially in cases of wind variation and/or multiple fires  
345 such as for the peaks monitored on April 6 (blue shaded region in Fig. 5a) and April 7, 2021 (yellow shaded region in  
346 Fig. 5a). Since there are multiple fires on the Fort all in the same southern direction relative to the trailer, the exact  
347 source cannot be determined solely based on wind vectors from RAWS data. In these cases, HYSPLIT back  
348 trajectories help to pinpoint the exact fire or fires contributing to the smoke event observed. In both cases on April 6  
349 (blue shaded region in Fig. 5a) and April 7, 2021 (yellow shaded region in Fig. 5a), the closer fire was the source of  
350 smoke as shown in Fig. 5e and 5f.

### 351 3.4. Determining smoke age



352 The physical age of smoke is the time it takes the smoke to be transported from the source to the monitoring  
353 sites. Following the concept presented for source identification, the transport time of smoke is estimated by averaging  
354 wind speed over the period for the smoke to travel from the fire to the measurements site, determined by iteration  
355 (mean wind speed recalculated with new transport time, until convergence). A detailed example on using average  
356 wind vector in estimating the physical age of smoke is provided in the Supplemental section S.1. The age was also  
357 determined from the HYSPLIT back trajectories as the time when the lowest trajectory intersects the source of smoke  
358 identified.

359 For the three events discussed in Fig. 5, physical ages estimated using the wind vector averaged from  
360 observed RAWS wind data are 75, 14, and 162 minutes for April 6 (blue shading), 7 (yellow shading) and 8 (green  
361 shading), 2021 events respectively. For the same events and using HYSPLIT trajectories closest to the surface and  
362 passing through the identified sources, ages were estimated as 130, 10, and 40 minutes respectively. Based on our  
363 analysis, April 6 (blue shading) stands out as the only case where the HYSPLIT age exceeds that estimated using the  
364 mean wind vector for the same fire source. The substantial difference between modeled and observed winds suggests  
365 that relying on the wind vector based on observed winds is more reliable in this instance. For all the smoke plumes  
366 identified, the age of smoke estimated based on HYSPLIT back trajectories ranged from 10 minutes (single timestep  
367 of trajectory) to 6 hours (36 timesteps), and from a few minutes to 8 hours based on average wind vector method  
368 (Table S9). A comparison summary between wind speeds observed by the RAWS and those modeled by WRF during  
369 all the events identified in 2021 and 2022 at the main trailer is shown in Fig. 6a. The observed weak correlation ( $r^2 =$   
370  $0.29$ ) could be due to several factors. For the wind vector analysis, observed winds are measured at one location and  
371 2 meters above ground level with a single monitor, which does not accurately represent the wind patterns along the  
372 entire smoke transport path. On the other hand, WRF simulates winds for 34 layers at different altitudes from 10 m,  
373 being the lowest, to levels higher than the PBL. HYSPLIT applies bilinear interpolation to the data from WRF for the  
374 10 trajectories that it calculates, introducing additional uncertainty to the wind patterns used in the simulations.  
375 Although the comparison between ages estimated based on the two different methods resulted in reasonable correlation  
376 ( $r^2=0.59$ ), the slope clearly indicates a significant higher estimation of age when using the wind vector method,  
377 particularly for more aged smoke events, as shown in Fig. 6b, where ages from the two methods show stronger  
378 agreement for fresh smoke. This can be attributed, in many cases, to the uncertainty in observed winds during low-  
379 speed wind conditions, the measurement being far from where winds are observed (RAWS), and most importantly  
380 that RAWS measures winds at 2 m above ground level whereas smoke transport happens at higher altitudes with  
381 stronger winds. There are additional discrepancies resulting from wind variation at each altitude at which HYSPLIT  
382 is running.

### 383 3.5. Limitations of the fixed site method

384 The goal of this project is to study the emissions and evolution of smoke from prescribed fires and provide  
385 data to test model simulations. Some limitations and challenges are associated with our approach of collecting data  
386 from a network of fixed sites.

387 *Identification of burning regions:* First, due to the limitations of satellite fire detection, some fires were not  
388 seen in FIRMS satellite detection data but were subsequently identified from the fire management report, such as the



389 prescribed fires on March 23, 2021, shown in Fig. S6a. The 20-minute averaged  $PM_{2.5}$  mass concentration at the trailer  
390 increased to  $74.8 \mu\text{g m}^{-3}$ , and to  $47.8 \mu\text{g m}^{-3}$  hourly average at the EPD site located off-base at the Columbus Airport  
391 in the afternoon of March 23, 2021 as shown in the time series of Fig. S6b. This increase was accompanied by an  
392 elevation in the levels of CO,  $PM_{2.5}$  mass, BC, and BrC measured at the trailer. This is an example of burning on the  
393 Fort likely affecting the nearby urban population. Prevailing winds were from the southeast at the time of the smoke  
394 event, as can be seen from the wind vectors presented on the same time series in Fig. S6b. However, FIRMS satellite  
395 data showed no hotspots on the Fort during the entire day. After checking the fire management report for 2021,  
396 prescribed burns for 3 units located in the east central part of the Fort at distances ranging from 8.1 to 14.7 miles from  
397 the trailer were identified. Looking at either the wind vector at the time of the peak or the HYSPLIT back trajectories,  
398 the source of the smoke event identified on March 23, 2021 matches the closer prescribed burn conducted on the Fort.

399 Another issue with this approach is that relying only on data from the burning authorities at Fort Moore can,  
400 in some cases, be insufficient due to the lack of information about fires taking place off-base by landowners, such as  
401 the off-base fire seen on FIRMS during three overpasses of satellites at 12:38, 13:54, and 14:42 (Fig. S7a). On May  
402 9, 2022 at 16:30, monitored species increased at the main trailer and 20 minutes average of  $PM_{2.5}$  mass reached  $52.3$   
403  $\mu\text{g m}^{-3}$  (Fig. S7b). The Fort's Fire Management reported no prescribed fires and one wildfire in the southern part of  
404 the base with an indication of zero probability of smoke from that fire reaching the trailer based on wind patterns.  
405 Based on both wind vectors and HYSPLIT simulations, the source of the event was identified as an off-base fire  
406 detected to the northeast of Fort Moore. The same smoke event was also observed at multiple trailers operating at the  
407 time and will be discussed more in the following section.

408 *Identifying a specific fire impacting the site when multiple burning is occurring:* When multiple fires are  
409 taking place simultaneously in varying wind conditions it can be difficult identifying the specific fire impacting the  
410 site, which can lead to uncertainty in the smoke age. This occurred in smoke detected around midnight on March 14,  
411 2022 (see Fig. S8a). Relying on wind data, the smoke source is likely one or more of the fires on the east and/or  
412 southeast side of the base with a zero probability of it being one of the fires in the northern part of the base. HYSPLIT  
413 may help in narrowing down the possibilities of the smoke source (Fig. S8b), but there is still uncertainty in linking  
414 the specific fire to the observed event.

415 When several burning units are in close proximity and near the measurement site, identifying the specific  
416 source and smoke age can also be difficult (for example see Fig. S9). In this case burning in three units indicated by  
417 the Fort's Fire Management occurred at the same time close to each other and the trailer (distances of 0.6, 1.4, and 2.2  
418 miles from the trailer). HYSPLIT trajectory at lowest altitude passes near (to the east), but not over the prescribed  
419 fires. Wind direction at the time of the event suggest influence from a minor portion from the northern part of the fire.

420 We note that there is no direct correlation between the amount of smoke reaching the trailer, i.e., measured  
421 species concentrations, and the distance of the fire from the monitoring site. The relation depends on the smoke  
422 transport and dispersion that may allow smoke to either directly hit the measuring site, partially reach the measuring  
423 site, or pass above the trailer with little or no smoke detection by the monitors. To illustrate this, we compare three  
424 case studies. Looking again at the smoke event of February 11, 2022 shown in Fig. S9, smoke reaching the trailer  
425 from 0.6 to 2.2 miles fires resulted in a 20-minute maximum  $PM_{2.5}$  mass of  $62.8 \mu\text{g m}^{-3}$  and CO concentration of 1.3



426 ppm at 13:30. On February 12, 2022 (Fig. S10 a and b), smoke from burns of units at distances 4.3 to 4.6 miles from  
427 the trailer, caused an increase in 20-minute  $PM_{2.5}$  mass concentration to  $60 \mu\text{g m}^{-3}$  and CO to 0.9 ppm at 13:50, whereas  
428 on the night of April 4, 2022 until the morning of April 5, 2022 (Fig. S10 c and d), smoke from fires 3.8 and 3.9 miles  
429 from the trailer, caused an increase of 20-minute  $PM_{2.5}$  mass concentration to  $319 \mu\text{g m}^{-3}$  and CO to 3.0 ppm at 1:10  
430 over a longer smoke monitoring period. The much higher  $PM_{2.5}$  mass concentrations measured on April 4, 2022  
431 suggests that the trailer received a more direct smoke hit on that day than on February 11, 2022 or February 12, 2022,  
432 despite the fire being closer on February 11 and having a very similar distance to the one detected on February 12.  
433 This can also be attributed to the much lower nighttime PBL on April 4, which was 9.75 m and caused all HYSPLIT  
434 trajectories to overlap as shown in Fig. 12d. Higher PBL of 1645 and 1305 m during the daytime on February 11 and  
435 12, respectively, favored more vertical dispersion of smoke.

436 *Smoke not detected although regions of burning identified:* On certain days, based on the wind data and the  
437 information presented in the fire management report, it appears likely that smoke from the fires at the base should  
438 reach specific monitoring sites. However, during those instances, such as the situation on February 15, 2022 shown in  
439 Fig. 7, no significant smoke peaks were detected. To explain this outcome, two HYSPLIT forward trajectory  
440 simulations were run. The simulations show that if the fire starts at 10:00, the smoke will not intercept the monitor,  
441 but if it starts at 11:00, the smoke at higher altitudes has a slight chance of reaching the monitor. Overall, regardless  
442 of wind direction favoring smoke transport to monitors, other factors like dispersion and smoke plume behavior, such  
443 as lofting, play a significant role in the transport process.

### 444 **3.6 Advantages of multiple monitoring sites**

445 There are distinct advantages of setting up multiple measuring sites and studying smoke over an extended  
446 period. First, it helps capture more smoke events, as seen during the 2022 study in comparison with that in 2021 when  
447 a single trailer was used. It minimizes issues with predicting downwind locations and is not affected by uncertainty in  
448 planned burning locations and times. Second, it reduces the labor and time required for relocating a single trailer and  
449 setting it up several times throughout a prescribed burning period where burning occurs over different regions. Third,  
450 it provides high spatial resolution and occasionally smoke from the same fire is detected at several sites, which can be  
451 useful in studying smoke chemical evolution with higher certainty than studies of multiple plumes of varying ages  
452 measured on different days.

453 An example of the same fire detected at several sites is shown in Fig. 8. On May 9, 2022, each of T1291,  
454 T1292, Main Trailer, and T1293 detected an off-base fire taking place approximately 11 miles to the north northeast  
455 of the base, as shown in Fig. 8a. T1291, the closest trailer to the fire, measured  $PM_{2.5}$  mass and CO peaks at 15:10.  
456 The time series of species measured in the various trailers is shown in Fig. 8. Subsequent peaks in  $PM_{2.5}$  mass, CO,  
457 BC, and  $O_3$  concentrations were recorded at T1292, at 15:50, then at the main trailer at 16:30, and finally at T1293,  
458 the furthest trailer from the fire, at 18:10 local time. For  $O_3$ , note the  $O_3$  enhancement ( $\Delta O_3$ ) superimposed on the  
459 diurnal  $O_3$  trend. The ages of the smoke detected based on wind vector analysis were 266, 296, 330 and 480 minutes,  
460 for the various trailers. The differences in peak concentrations can be due to a number of factors, including changes  
461 in fire emissions with time, extent of plume dilution with distance from the fire and changes in what portions of the  
462 plume were measured due to changes in winds. Wind vectors are shown at the top of plots in Fig. 8. Wind direction





463 and speed varied during the period when the plumes were recorded; wind direction was between 52° and 86° from  
464 11:00 till 14:00 and speeds between 3 and 7 mph on May 9, 2022. A shift in wind direction to 348° at a speed of 4  
465 mph happened at 15:00. Then, the wind direction fluctuated between 11° and 44°, before wind speed decreased to 0  
466 mph at 20:00 and remained calm until the morning of May 10, 2022. Normalizing these plume data by a stable smoke  
467 tracer, such as CO, can account for some of these factors when comparing emissions and evolution of various plume  
468 properties.

### 469 3.7 PM<sub>2.5</sub> emissions

470 We used the normalized excess mixing ratio (NEMR) to study the emissions of PM<sub>2.5</sub> species and their  
471 evolution in the various measured smoke plumes. The NEMRs determined from the linear regression slopes of PM<sub>2.5</sub>  
472 species (mass concentration, BC concentration, BrC absorption versus CO, with backgrounds subtracted) and  
473 correlation values ( $r^2$ ) for all smoke events are summarized in Table 1. PM<sub>2.5</sub> mass concentration NEMRs from other  
474 studies are summarized in Table S10.

475 The NEMR of fresh smoke near a fire is interpreted as an emission ratio (ER), assuming the smoke has  
476 undergone limited chemical and/or physical changes. ERs based on NEMRs are widely used (Liu et al., 2017b; Collier  
477 et al., 2016; Burling et al., 2011; Gkatzelis et al., 2024). They are compiled in reviews and emission inventories for  
478 ambient (Andreae, 2019; Prichard et al., 2020) and laboratory fire studies (Yokelson et al., 2013), and for evaluating  
479 or making model predictions (Xiu et al., 2022; Jaffe et al., 2022).

480 By focusing on fresh smoke (age less than 1 hour), the emissions ratios (ER) of the prescribed fires can be  
481 estimated and compared to those from other studies. The PM<sub>2.5</sub> mass concentration ER ranged between 0.04 and 0.18  
482  $\mu\text{g m}^{-3} \text{ppb}^{-1}$  and is shown in Fig. 9. These ERs are comparable to other prescribed fires measured at both ground level  
483 (Alves et al., 2010; Desservettaz et al., 2017; Korontzi et al., 2003; Balachandran et al., 2013) and aloft in airborne  
484 studies (Sinha et al., 2003; Yokelson et al., 2011; Akagi et al., 2012; Burling et al., 2011; May et al., 2014; Yokelson  
485 et al., 2009; Gkatzelis et al., 2024) that span a large range of burning conditions and fuels (details are provided in  
486 Table S10). The mean PM<sub>2.5</sub> mass concentration ER for our data is  $0.117 \pm 0.045 \mu\text{g m}^{-3} \text{ppb}^{-1}$  and that of these other  
487 prescribed fire studies are  $0.098 \pm 0.034 \mu\text{g m}^{-3} \text{ppb}^{-1}$  for ground-based and  $0.115 \pm 0.086 \mu\text{g m}^{-3} \text{ppb}^{-1}$  for airborne  
488 measurements. There is substantial and similar variability in the ground-based measurements of proscribed fire ERs  
489 in this study relative to other studies. However, some airborne-measured prescribed fires have reported substantially  
490 higher ERs (Fig. 9). Smoke transported for 10 minutes from the Blackwater river state forest prescribed fire reported  
491 by Gkatzelis et al. had an ER of  $0.462 \mu\text{g m}^{-3} \text{ppb}^{-1}$  (Gkatzelis et al., 2024) and Burling et al. reported an ER of  $0.399$   
492  $\mu\text{g m}^{-3} \text{ppb}^{-1}$  for the Bear Pen prescribed fire in NC (Burling et al., 2011). Figure 9 also shows comparisons with  
493 wildfires reported in other studies (Liu et al., 2017b; Collier et al., 2016; Palm et al., 2020; Gkatzelis et al., 2024).  
494 Wildfire PM<sub>2.5</sub> mass ERs are significantly higher than ERs for prescribed fires in this work, with ER ranges between  
495 0.04 and  $0.43 \mu\text{g m}^{-3} \text{ppb}^{-1}$  and a mean of  $0.264 \pm 0.091 \mu\text{g m}^{-3} \text{ppb}^{-1}$  for wildfires, and the difference is statistically  
496 significant (two-tailed p value is  $< 0.0001$ ). Lower PM<sub>2.5</sub> mass ERs from smaller prescribed fires has been noted in  
497 other studies (Liu et al., 2017b) and supports utilizing prescribed burning as a land management tool to limit wildfires.  
498 However, differences in altitude at which the measurements were made may have some effect on ERs. Selimovic et



499 al. (Selimovic et al., 2019) noted that the  $PM_{2.5}/CO$  in ground-level smoke was about half of that observed from aloft  
500 apparently due to reduction in aerosol mass from evaporation of semi-volatile aerosol particle components resulting  
501 from higher surface temperatures compared to aloft. However, when comparing ERs of prescribed fires in ground  
502 versus airborne studies of prescribed fires, shown in Fig. 9, the difference is not significant ( $p$  value is 0.435).

503 This analysis assumes no significant changes in  $PM_{2.5}$  mass for smoke less than 1 hour old. We have seen  
504 that smoke detected in the afternoon can have enhanced  $O_3$  concentrations, which may also lead to secondary aerosol  
505 formation. Smoke plumes with enhanced  $O_3$  are identified in the ERs shown in Fig. 9 and indicate no bias within the  
506 range of ERs recorded, suggesting possible secondary aerosol formation within the first hour following emissions  
507 does not contribute to the ER variability. We also did not find evidence of ERs depending on time of day. No difference  
508 was seen between ERs for fires that started on the same day of measurement (i.e., all detected after 9:00 and before  
509 17:00), and those detected at night, after 17:00, or early in the morning corresponding to fires that started the day  
510 before the measurement, but still were estimated to correspond to smoke less than one hour old.

511 We also determined the ERs for BC and BrC. BC ERs were in the range of  $0.008\text{--}0.022 \mu\text{g m}^{-3} \text{ppb}^{-1}$  with a  
512 mean value of  $0.014 \pm 0.004 \mu\text{g m}^{-3} \text{ppb}^{-1}$ , which are within the range of NEMRs reported in other studies;  $0.006 \mu\text{g}$   
513  $\text{m}^{-3} \text{ppb}^{-1}$  for prescribed burns in southern African savanna forests (Sinha et al., 2003),  $0.020 \mu\text{g m}^{-3} \text{ppb}^{-1}$  for rBC  
514 (refractory BC) for prescribed burns of California chaparral forests (Akagi et al., 2012),  $0.022 \mu\text{g m}^{-3} \text{ppb}^{-1}$  for  
515 chaparral forests (May et al., 2014),  $0.006 \mu\text{g m}^{-3} \text{ppb}^{-1}$  for fires in Montane ecosystems (May et al., 2014), 0.018 for  
516 coastal plain ecosystems in South Carolina (May et al., 2014), and  $0.004 \mu\text{g m}^{-3} \text{ppb}^{-1}$  for large wildfires over the  
517 western US measured during FIREX (Gkatzelis et al., 2024).

518 The BrC ERs of fresh smoke events ranged between  $0.151$  and  $0.689 \text{Mm}^{-1} \text{ppb}^{-1}$  with a mean  $\pm$  standard  
519 deviation of  $0.442 \pm 0.157 \text{Mm}^{-1} \text{ppb}^{-1}$ . There is limited published data on BrC ERs and NEMRs from prescribed fires  
520 and the measurement techniques of BrC vary between studies. Liu et al. (Liu et al., 2016) reported aircraft  
521 measurements of BrC at 365 nm inferred from PSAP absorption coefficients measured at two wavelengths (470 and  
522 532 nm) with an ER of  $0.223 \pm 0.053 \text{Mm}^{-1} \text{ppb}^{-1}$  for fresh agricultural fires in the southeastern US, which is lower  
523 than our mean, but falls within the range of values we observed. For large wildfires measured over the western US,  
524 Zeng et al. (Zeng et al., 2022) found for Photoacoustic Spectroscopy (PAS) measurements of BrC at a wavelength of  
525 405 nm, the ER was  $0.131 \pm 0.001 \text{Mm}^{-1} \text{ppbv}^{-1}$  in plumes  $< 2$  hours old. These values are in the range we recorded,  
526 but the BrC ER for the prescribed fires of this study are more variable.

### 527 **3.8 NEMRs of all smoke events and their change with smoke age**

528 Here we assess the overall variability in NEMRs for  $PM_{2.5}$  mass concentrations, BC mass concentrations,  
529 BrC absorption coefficients, and AAEs from all the smoke events (including ages less than 1 hour) and assess possible  
530 trends with smoke plume age. In this analysis, the observed changes with age are a combination of variability in  
531 emissions and evolution of the aerosol since it is not a Lagrangian experiment, meaning that we are not continuously  
532 tracking a specific air mass containing smoke particles over time.  $PM_{2.5}$  mass concentration NEMRs varied between  
533  $0.04$  and  $0.47 \mu\text{g m}^{-3} \text{ppb}^{-1}$  for all reported events with a mean  $\pm$  standard deviation of  $0.155 \pm 0.076 \mu\text{g m}^{-3} \text{ppb}^{-1}$   
534 (median is  $0.138 \mu\text{g m}^{-3} \text{ppb}^{-1}$ ). BC NEMRs ranged between  $0.005$  and  $0.024 \mu\text{g m}^{-3} \text{ppb}^{-1}$  with a mean value of  $0.013$





535  $\pm 0.005 \mu\text{g m}^{-3} \text{ppb}^{-1}$ . BrC NEMRs ( $\Delta\text{BrC}/\Delta\text{CO}$ ) varied between 0.133 to 1.550  $\text{Mm}^{-1} \text{ppb}^{-1}$ . (Note that data collected  
536 on April 21, 2022 at trailer 1293 is an outlier with exceptionally high ERs for  $\text{PM}_{2.5}$  mass concentration and BrC  
537 absorption coefficient. The ER for BC mass concentration, while elevated, falls within the observed range. This event  
538 corresponds to smoke from an identified prescribed fire at the Fort and has a relatively low  $\Delta\text{CO}$  of 66.1 ppm, which  
539 is unexpected given the burn's proximity and the wind conditions on that day, causing ERs to be significantly higher).  
540 The NEMRs are given in Table 1 for all smoke events data and plotted in Fig. 10 as a function of estimated smoke  
541 age determined from the wind vector and HYSPLIT analysis. From these plots we assess if there is any systematic  
542 evolution of the  $\text{PM}_{2.5}$  mass, BC and BrC.

543 *Changes in  $\text{PM}_{2.5}$  Mass Concentration NEMR with smoke age:* From Fig. 10a,  $\text{PM}_{2.5}$  mass concentration  
544 NEMR shows substantial variability at all ages with no significant statistical difference or clear trend, however, NEMR  
545 tends to be lower for fresh smoke events ( $\leq 1$  hour old) versus more aged plumes, possibly from secondary aerosol  
546 formation. Considering only smoke plumes in which  $\text{O}_3$  enhancements were observed (i.e., smoke measured between  
547 12:00 and 18:00),  $\text{PM}_{2.5}$  mass concentration NEMR consistently increases with physical age ( $r^2=0.65$ ), evidence of  
548 secondary aerosol formation through a photochemical process that directly involve  $\text{O}_3$ , or some other related oxidant,  
549 (e.g., OH) (Liu et al., 2016).

550 A range of results for changes in  $\text{PM}_{2.5}$  mass concentration NEMRs in wildland fires have been observed in  
551 other studies, including systematic increases, little change, or decreases with smoke age. To the best of our knowledge,  
552 no ground-based studies have been conducted on the evolution of smoke from prescribed fires, but frequent airborne  
553 studies have investigated prescribed and wildland smoke aging because of the ability to spatially characterize a single  
554 plume. While studying two prescribed fires in SC, May et al. (May et al., 2015) observed no statistically significant  
555 net change in OA NEMRs near the source and downwind for smoke transported for  $\leq 1.5$  hours. One of the two fires  
556 was studied for longer, and results showed downwind OA NEMRs over 2 to 5 hours of transport significantly lower  
557 than the NEMRs at the source, suggesting a net loss of emitted OA. Also, a decrease in OA/CO from 0.057 to 0.046  
558  $\mu\text{g m}^{-3} \text{ppb}^{-1}$  was reported after 4 hours in an airborne study of an 81 hectare prescribed fire in chaparral fuels on the  
559 central coast of California (Akagi et al., 2012). In contrast, an airborne study of 20 deforestation and crop residue fires  
560 on the Yucatan peninsula, reported an increase in  $\text{PM}_{2.5}$  NEMRs by a factor of 2.6 (NEMR increased from 0.072 to  
561  $0.187 \mu\text{g m}^{-3} \text{ppb}^{-1}$ ) in the first 1.4 hours due to rapid secondary formation of organic and inorganic aerosol (Yokelson  
562 et al., 2009). For wildfires, Collier et al. (Collier et al., 2016) found increases, little change, and decreases with smoke  
563 age in different wildfire plumes measured in Oregon. For the selected large wildfires in the western US in summer,  
564 Palm et al. (Palm et al., 2020) reported that the OA NEMR remained almost constant at a value of  $\sim 0.25 \mu\text{g m}^{-3} \text{ppb}^{-1}$   
565 as the plume aged from 20-50 minutes to 6 hours. Gkatzelis et al. reported the NEMRs of some plumes that were  
566 more than an hour old and are shown in Table S10 with their corresponding physical age (Gkatzelis et al., 2024). For  
567 the same fire (William's flat), the NEMR was  $0.331 \mu\text{g m}^{-3} \text{ppb}^{-1}$  at physical age of 15 minutes that increased to  $0.524$   
568  $\mu\text{g m}^{-3} \text{ppb}^{-1}$  at 102 minutes (Gkatzelis et al., 2024). Similar increase for the Castle fire was seen where the NEMRs  
569 reported are 0.204, 0.244, and  $0.463 \mu\text{g m}^{-3} \text{ppb}^{-1}$  at 25, 27, and 153 minutes respectively. For another fire (Horsefly),  
570 the NEMR was  $0.398 \mu\text{g m}^{-3} \text{ppb}^{-1}$  at a physical age of 65 minutes and remained at a similar value of  $0.391 \mu\text{g m}^{-3}$



571  $\text{ppb}^{-1}$  at 104 minutes. On average, the mean NEMRs for plumes of physical age less than one hour, reported in their  
572 study, was  $0.218 \pm 0.110$ . This value is lower than that of plumes older than one hour, which have a mean value of  
573  $0.391 \pm 0.131$  (Gkatzelis et al., 2024). Overall, we find no trends in our data when considering all the smoke plumes  
574 detected, but for periods of expected photochemical activity we observe consistent evidence for aerosol formation  
575 with plume age, which might be attributed to the optically thin smoke that allows photochemistry throughout the  
576 plume compared to large optically thick wildfires that leads to more complex photochemistry within the plume  
577 (Decker et al., 2021a).

578 We examined other factors that may contribute to variability of  $\text{PM}_{2.5}$  mass NEMRs. No significant difference  
579 was observed between on-base and off-base sources of smoke. Mean  $\text{PM}_{2.5}$  mass NEMR of smoke originating from  
580 outside the base is  $0.208$  (range  $0.112\text{--}0.277 \mu\text{g m}^{-3} \text{ppb}^{-1}$ ), compared to  $0.147 \mu\text{g m}^{-3} \text{ppb}^{-1}$  (range  $0.042\text{--}0.466 \mu\text{g}$   
581  $\text{m}^{-3} \text{ppb}^{-1}$ ) for on base burning, which is not statistically different (two tailed p-value is 0.076). Satellite images do not  
582 show any visible differences in vegetation between the forested areas burnt on and off the base. Additionally, no  
583 further information regarding the fuel types in the off-base lands could be obtained. Just like no detected differences  
584 being observed between day/night  $\text{PM}_{2.5}$  mass concentration ERs, there was no significant difference (p-value is 0.169)  
585 between smoke plumes of all ages measured during the day corresponding to fires occurring within a few hours from  
586 starting the burn (after 9:00 and before 17:00) (mean NEMR =  $0.178 \mu\text{g m}^{-3} \text{ppb}^{-1}$ ) and those monitored at night and  
587 early in the morning corresponding to fires starting the day before (after 17:00) (mean NEMR =  $0.137 \mu\text{g m}^{-3} \text{ppb}^{-1}$ ),  
588 in contrast to an observed trend of  $\text{PM}_{2.5}$  mass NEMR with age for smoke with  $\text{O}_3$  enhancement. This may suggest  
589 little night-time secondary aerosol formation (Brown et al., 2013), but a more focused analyses is needed to better  
590 assess possible evidence for secondary aerosol formation. No correlation was observed between  $\text{PM}_{2.5}$  mass NEMRs  
591 and relative humidity ( $r^2=0.08$ ) or fuel moisture data ( $r^2=0.04$ ) for the smoke events in this study (Fig. S12). A weak  
592 positive correlation between air temperature and  $\text{PM}_{2.5}$  mass NEMRs was observed, with an  $r^2$  of 0.14 for all smoke  
593 events and  $r^2$  of 0.44 for fresh smoke events. Many factors could cause variability in  $\text{PM}_{2.5}$  mass NEMRs, but no single  
594 factor could be identified when all data from this study is grouped together.

595 *Changes in BC and BrC NEMR with smoke age:* BC and BrC NEMRs versus age are shown in Fig. 10b and  
596 10c with periods of  $\text{O}_3$  enhancements identified. No trend in BC NEMRs with age is observed, as expected, since BC  
597 is primarily emitted and largely nonvolatile. Lack of a trend supports this analysis approach and all the BC measured  
598 in events largely reflects BC variability in emissions relative to CO. BrC NEMRs are also highly variable and have  
599 no trend with age for all the data or just the periods of  $\text{O}_3$  enhancements. Since BrC can be both primary and secondary,  
600 is semi-volatile, and undergoes photo-bleaching, a range of results on BrC evolution has been observed in past studies  
601 (Zhong and Jang, 2014; Saleh et al., 2013; Liu et al., 2016). Like BC, a similar large variability, with no trend, in BrC  
602 NEMRs with ages up to 8 hours has been observed for wildfires in the western US (Zeng et al., 2022; Sullivan et al.,  
603 2022; Palm et al., 2020) whereas in some cases consistent loss (bleaching) of BrC has been reported (Forrister et al.,  
604 2015). Optical properties of absorptive aerosol spectral properties characterized by AAE are shown in Fig. 11 as a  
605 function of age. Total absorption AAE values from the two trailers with 7-wavelength aethalometers (i.e., BC+BrC  
606 measured by the aethalometer) varied between 1.31 and 3.32 (mean  $\pm$  stdev of  $1.89 \pm 0.23$ ) and between 3.19 and 7.43



607 (mean =  $5.00 \pm 0.89$ ) for BrC only. AAEs have no trend with age for either fresh smoke plumes or periods of O<sub>3</sub>  
608 enhancement. While our total AAE values are similar (Zeng et al., 2022; Strand et al., 2016; Marsavin et al., 2023) or  
609 sometimes lower (Liu et al., 2016; Forrister et al., 2015) than those in other biomass burning studies, it is indicative  
610 of the presence of BrC in the smoke plumes studied. As for BrC AAEs, our reported values are significantly higher  
611 than those reported for western wildfires, where BrC determined from the PAS had an AAE of  $2.07 \pm 1.01$  (Zeng et  
612 al., 2022), indicating difference in BrC optical properties or with instrumentation, which needs further investigation.

#### 613 4. Conclusion

614 We describe a ground-based measurement method for characterizing smoke from prescribed fires based on  
615 continuous monitoring at multiple sites for an extended period in a regularly burned region. The method was successful  
616 in capturing a significant number of smoke events (64). Source and age for each smoke plume detected was  
617 determined. This allowed us to match 95 % of the identified events to their corresponding source and to calculate the  
618 estimated transport time of smoke from source to monitors. These data were used to characterize emissions and  
619 evolution of key smoke parameters through calculation of normalized excess mixing ratios (NEMRs), with CO as the  
620 conservative parameter. Overall, PM<sub>2.5</sub> mass concentration NEMRs ( $\Delta\text{PM}_{2.5} \text{ mass}/\Delta\text{CO}$ ) ranged between 0.04 and  
621  $0.47 \mu\text{g m}^{-3} \text{ ppb}^{-1}$  with a study mean of  $0.155 \pm 0.076 \mu\text{g m}^{-3} \text{ ppb}^{-1}$  (median is  $0.138 \mu\text{g m}^{-3} \text{ ppb}^{-1}$ ). For plumes less  
622 than 1 hour old the PM<sub>2.5</sub> mass concentration NEMRs were interpreted as a characteristic of the fire's emissions.  
623 Emissions ratios for fires of this study ranged between 0.042 and  $0.176 \mu\text{g m}^{-3} \text{ ppb}^{-1}$  with a mean of  $0.117 \pm 0.045 \mu\text{g}$   
624  $\text{m}^{-3} \text{ ppb}^{-1}$  (median is  $0.121 \mu\text{g m}^{-3} \text{ ppb}^{-1}$ ). These emissions estimates are in the range reported in other ground-based  
625 studies for a range of fires and fuels but are lower than what has been reported for wildfire smoke measured from  
626 aircraft at higher altitudes. BC and BrC NEMRs and emission ratios are also reported. An analysis of PM<sub>2.5</sub> mass and  
627 BrC NEMRs changes with smoke age showed no consistent trends for all combined smoke plumes. However, PM<sub>2.5</sub>  
628 mass NEMRs did increase with age for smoke detected in the afternoon in plumes where O<sub>3</sub> enhancements were  
629 observed, indicating combined secondary O<sub>3</sub> and particle mass formation. This was not observed for BrC NEMRs.  
630 This data set will be used to assess models predicting the impact of prescribed fires on air quality to enhance the use  
631 of prescribed burning in land management practices by minimizing impacts on populations.

#### 632 5. Competing interests

633 The contact author has declared that none of the authors has any competing interests.

#### 634 6. Acknowledgements

635 We thank Fort Moore authorities for hosting the field study, and to the members of the Natural Resources Management  
636 Branch for sharing information about the burns. REA, DJT, GH and RJW were supported by the United States Army  
637 Corps of Engineers under contract W912HQ-20-C-0019. ZL, YH, and MTO were supported by the Strategic  
638 Environmental Research and Development Program (SERDP) through project RC20-1047.

639 **Author contribution:** REA and RJW wrote the paper. RJW, LGH, DJT, and MTO designed the experiment. REA  
640 and DJT collected the data. REA, ZL, DJT, and RJW analyzed data. REA and ZL worked on the HYSPLIT analysis.  
641 All authors reviewed and provided comments for the paper.

642 **Data availability:** Data are available in a publicly accessible repository: <https://doi.org/10.5281/zenodo.11222295>.



643 **References**

- 644 Akagi, S. K., Craven, J. S., Taylor, J. W., McMeeking, G. R., Yokelson, R. J., Burling, I. R., Urbanski, S. P., Wold,  
645 C. E., Seinfeld, J. H., Coe, H., Alvarado, M. J., and Weise, D. R.: Evolution of trace gases and particles emitted by a  
646 chaparral fire in California, *Atmos. Chem. Phys.*, 12, 1397–1421, <https://doi.org/10.5194/acp-12-1397-2012>, 2012.
- 647 Akagi, S. K., Burling, I. R., Mendoza, A., Johnson, T. J., Cameron, M., Griffith, D. W. T., Paton-Walsh, C., Weise,  
648 D. R., Reardon, J., and Yokelson, R. J.: Field measurements of trace gases emitted by prescribed fires in  
649 southeastern US pine forests using an open-path FTIR system, *Atmos. Chem. Phys.*, [https://doi.org/10.5194/acp-14-](https://doi.org/10.5194/acp-14-199-2014)  
650 199-2014, 2014.
- 651 Alves, C. A., Gonçalves, C., Pio, C. A., Mirante, F., Caseiro, A., Tarelho, L., Freitas, M. C., and Viegas, D. X.:  
652 Smoke emissions from biomass burning in a Mediterranean shrubland, *Atmos. Environ.*, 44, 3024–3033,  
653 <https://doi.org/10.1016/j.atmosenv.2010.05.010>, 2010.
- 654 Andreae, M. O.: Emission of trace gases and aerosols from biomass burning – an updated assessment, *Atmos.*  
655 *Chem. Phys.*, 19, 8523–8546, <https://doi.org/10.5194/acp-19-8523-2019>, 2019.
- 656 Balachandran, S., Pachon, J. E., Lee, S., Oakes, M. M., Rastogi, N., Shi, W., Tagaris, E., Yan, B., Davis, A., Zhang,  
657 X., Weber, R. J., Mulholland, J. A., Bergin, M. H., Zheng, M., and Russell, A. G.: Particulate and gas sampling of  
658 prescribed fires in South Georgia, USA, *Atmos. Environ.*, 81, 125–135,  
659 <https://doi.org/10.1016/j.atmosenv.2013.08.014>, 2013.
- 660 Bell, M. L.: Ozone and Short-term Mortality in 95 US Urban Communities, 1987-2000, *JAMA*, 292, 2372,  
661 <https://doi.org/10.1001/jama.292.19.2372>, 2004.
- 662 Bond, T. C., Anderson, T. L., and Campbell, D.: Calibration and Intercomparison of Filter-Based Measurements of  
663 Visible Light Absorption by Aerosols, *Aerosol Sci. Technol.*, <https://doi.org/10.1080/027868299304435>, 1999.
- 664 Borchers-Arriagada, N., Bowman, D. M. J. S., Price, O., Palmer, A. J., Samson, S., Clarke, H., Sepulveda, G., and  
665 Johnston, F. H.: Smoke health costs and the calculus for wildfires fuel management: a modelling study, *Lancet*  
666 *Planet. Heal.*, [https://doi.org/10.1016/S2542-5196\(21\)00198-4](https://doi.org/10.1016/S2542-5196(21)00198-4), 2021.
- 667 Brown, S. S., Dubé, W. P., Bahreini, R., Middlebrook, A. M., Brock, C. A., Warneke, C., de Gouw, J. A.,  
668 Washenfelder, R. A., Atlas, E., Peischl, J., Ryerson, T. B., Holloway, J. S., Schwarz, J. P., Spackman, R., Trainer,  
669 M., Parrish, D. D., Fehsenfeld, F. C., and Ravishankara, A. R.: Biogenic VOC oxidation and organic aerosol  
670 formation in an urban nocturnal boundary layer: aircraft vertical profiles in Houston, TX, *Atmos. Chem. Phys.*, 13,  
671 11317–11337, <https://doi.org/10.5194/acp-13-11317-2013>, 2013.
- 672 Burling, I. R., Yokelson, R. J., Akagi, S. K., Urbanski, S. P., Wold, C. E., Griffith, D. W. T., Johnson, T. J.,  
673 Reardon, J., and Weise, D. R.: Airborne and ground-based measurements of the trace gases and particles emitted by  
674 prescribed fires in the United States, *Atmos. Chem. Phys.*, 11, 12197–12216, [https://doi.org/10.5194/acp-11-12197-](https://doi.org/10.5194/acp-11-12197-2011)  
675 2011, 2011.



- 676 Buysse, C. E., Kaulfus, A., Nair, U., and Jaffe, D. A.: Relationships between Particulate Matter, Ozone, and  
677 Nitrogen Oxides during Urban Smoke Events in the Western US, *Environ. Sci. Technol.*,  
678 <https://doi.org/10.1021/acs.est.9b05241>, 2019.
- 679 Christopher, S. A., Chou, J., Welch, R. M., Kliche, D. V., and Connors, V. S.: Satellite investigations of fire, smoke,  
680 and Carbon Monoxide during April 1994 MAPS mission: Case studies over tropical Asia, *J. Geophys. Res. Atmos.*,  
681 <https://doi.org/10.1029/97JD01813>, 1998.
- 682 Collier, S., Zhou, S., Onasch, T. B., Jaffe, D. A., Kleinman, L., Sedlacek, A. J., Briggs, N. L., Hee, J., Fortner, E.,  
683 Shilling, J. E., Worsnop, D., Yokelson, R. J., Parworth, C., Ge, X., Xu, J., Butterfield, Z., Chand, D., Dubey, M. K.,  
684 Pekour, M. S., Springston, S., and Zhang, Q.: Regional Influence of Aerosol Emissions from Wildfires Driven by  
685 Combustion Efficiency: Insights from the BBOP Campaign, *Environ. Sci. Technol.*, 50, 8613–8622,  
686 <https://doi.org/10.1021/acs.est.6b01617>, 2016.
- 687 Cubison, M. J., Ortega, A. M., Hayes, P. L., Farmer, D. K., Day, D., Lechner, M. J., Brune, W. H., Apel, E., Diskin,  
688 G. S., Fisher, J. A., Fuelberg, H. E., Hecobian, A., Knapp, D. J., Mikoviny, T., Riemer, D., Sachse, G. W., Sessions,  
689 W., Weber, R. J., Weinheimer, A. J., Wisthaler, A., and Jimenez, J. L.: Effects of aging on organic aerosol from  
690 open biomass burning smoke in aircraft and laboratory studies, *Atmos. Chem. Phys.*, [https://doi.org/10.5194/acp-11-](https://doi.org/10.5194/acp-11-12049-2011)  
691 12049-2011, 2011.
- 692 Decker, Z. C. J., Robinson, M. A., Barsanti, K. C., Bourgeois, I., Coggon, M. M., DiGangi, J. P., Diskin, G. S.,  
693 Flocke, F. M., Franchin, A., Fredrickson, C. D., Gkatzelis, G. I., Hall, S. R., Halliday, H., Holmes, C. D., Huey, L.  
694 G., Lee, Y. R., Lindaas, J., Middlebrook, A. M., Montzka, D. D., Moore, R., Neuman, J. A., Nowak, J. B., Palm, B.  
695 B., Peischl, J., Piel, F., Rickly, P. S., Rollins, A. W., Ryerson, T. B., Schwantes, R. H., Sekimoto, K., Thornhill, L.,  
696 Thornton, J. A., Tyndall, G. S., Ullmann, K., Van Rooy, P., Veres, P. R., Warneke, C., Washenfelder, R. A.,  
697 Weinheimer, A. J., Wiggins, E., Winstead, E., Wisthaler, A., Womack, C., and Brown, S. S.: Nighttime and daytime  
698 dark oxidation chemistry in wildfire plumes: an observation and model analysis of FIREX-AQ aircraft data, *Atmos.*  
699 *Chem. Phys.*, 21, 16293–16317, <https://doi.org/10.5194/acp-21-16293-2021>, 2021a.
- 700 Decker, Z. C. J., Wang, S., Bourgeois, I., Campuzano Jost, P., Coggon, M. M., DiGangi, J. P., Diskin, G. S., Flocke,  
701 F. M., Franchin, A., Fredrickson, C. D., Gkatzelis, G. I., Hall, S. R., Halliday, H., Hayden, K., Holmes, C. D., Huey,  
702 L. G., Jimenez, J. L., Lee, Y. R., Lindaas, J., Middlebrook, A. M., Montzka, D. D., Neuman, J. A., Nowak, J. B.,  
703 Pagonis, D., Palm, B. B., Peischl, J., Piel, F., Rickly, P. S., Robinson, M. A., Rollins, A. W., Ryerson, T. B.,  
704 Sekimoto, K., Thornton, J. A., Tyndall, G. S., Ullmann, K., Veres, P. R., Warneke, C., Washenfelder, R. A.,  
705 Weinheimer, A. J., Wisthaler, A., Womack, C., and Brown, S. S.: Novel Analysis to Quantify Plume Crosswind  
706 Heterogeneity Applied to Biomass Burning Smoke, *Environ. Sci. Technol.*, <https://doi.org/10.1021/acs.est.1c03803>,  
707 2021b.
- 708 Deng, A., Stauffer, D., Guadet, B., Dudhia, J., Hacker, J., Bruyere, C., Wu, W., Vandenberghe, F., Liu, Y., and  
709 Bourgeois, A.: A 1.9 Update on WRF-ARW End-to-End Multi-Scale FDDA System, in: In Proceedings of the  
710 WRF Users' Workshop, 2009.



- 711 Desservettaz, M., Paton-Walsh, C., Griffith, D. W. T., Kettlewell, G., Keywood, M. D., Vanderschoot, M. V., Ward,  
712 J., Mallet, M. D., Milic, A., Miljevic, B., Ristovski, Z. D., Howard, D., Edwards, G. C., and Atkinson, B.: Emission  
713 factors of trace gases and particles from tropical savanna fires in Australia, *J. Geophys. Res. Atmos.*, 122, 6059–  
714 6074, <https://doi.org/10.1002/2016JD025925>, 2017.
- 715 Forrister, H., Liu, J., Scheuer, E., Dibb, J., Ziemba, L., Thornhill, K. L., Anderson, B., Diskin, G., Perring, A. E.,  
716 Schwarz, J. P., Campuzano-Jost, P., Day, D. A., Palm, B. B., Jimenez, J. L., Nenes, A., and Weber, R. J.: Evolution  
717 of brown carbon in wildfire plumes, *Geophys. Res. Lett.*, 42, 4623–4630, <https://doi.org/10.1002/2015GL063897>,  
718 2015.
- 719 Giglio, L., Schroeder, W., Hall, J., and Justice, C.: MODIS Collection 6 and Collection 6.1 Active Fire Product  
720 User's Guide, Nasa, Version 1., 64, 2021.
- 721 Gkatzelis, G. I., Coggon, M. M., Stockwell, C. E., Hornbrook, R. S., Allen, H., Apel, E. C., Bela, M. M., Blake, D.  
722 R., Bourgeois, I., Brown, S. S., Campuzano-Jost, P., St. Clair, J. M., Crawford, J. H., Crouse, J. D., Day, D. A.,  
723 DiGangi, J. P., Diskin, G. S., Fried, A., Gilman, J. B., Guo, H., Hair, J. W., Halliday, H. S., Hanisco, T. F., Hannun,  
724 R., Hills, A., Huey, L. G., Jimenez, J. L., Katich, J. M., Lamplugh, A., Lee, Y. R., Liao, J., Lindaas, J., McKeen, S.  
725 A., Mikoviny, T., Nault, B. A., Neuman, J. A., Nowak, J. B., Pagonis, D., Peischl, J., Perring, A. E., Piel, F., Rickly,  
726 P. S., Robinson, M. A., Rollins, A. W., Ryerson, T. B., Schueneman, M. K., Schwantes, R. H., Schwarz, J. P.,  
727 Sekimoto, K., Selimovic, V., Shingler, T., Tanner, D. J., Tomsche, L., Vasquez, K. T., Veres, P. R., Washenfelder,  
728 R., Weibring, P., Wennberg, P. O., Wisthaler, A., Wolfe, G. M., Womack, C. C., Xu, L., Ball, K., Yokelson, R. J.,  
729 and Warneke, C.: Parameterizations of US wildfire and prescribed fire emission ratios and emission factors based on  
730 FIREX-AQ aircraft measurements, *Atmos. Chem. Phys.*, 24, 929–956, <https://doi.org/10.5194/acp-24-929-2024>,  
731 2024.
- 732 Hecobian, A., Zhang, X., Zheng, M., Frank, N., Edgerton, E. S., and Weber, R. J.: Water-soluble organic aerosol  
733 material and the light-absorption characteristics of aqueous extracts measured over the Southeastern United States,  
734 *Atmos. Chem. Phys.*, <https://doi.org/10.5194/acp-10-5965-2010>, 2010.
- 735 Huang, R., Hu, Y., Russell, A. G., Mulholland, J. A., and Odman, M. T.: The Impacts of Prescribed Fire on PM2.5  
736 Air Quality and Human Health: Application to Asthma-Related Emergency Room Visits in Georgia, USA, *Int. J.*  
737 *Environ. Res. Public Health*, 16, 2312, <https://doi.org/10.3390/ijerph16132312>, 2019.
- 738 Ichoku, C. and Kaufman, Y. J.: A method to derive smoke emission rates from MODIS fire radiative energy  
739 measurements, in: *IEEE Transactions on Geoscience and Remote Sensing*,  
740 <https://doi.org/10.1109/TGRS.2005.857328>, 2005.
- 741 Ichoku, C., Ellison, L. T., Yue, Y., Wang, J., and Kaiser, J. W.: Fire and Smoke Remote Sensing and Modeling  
742 Uncertainties, <https://doi.org/10.1002/9781119028116.ch14>, 2016.
- 743 Jaffe, D. A., O'Neill, S. M., Larkin, N. K., Holder, A. L., Peterson, D. L., Halofsky, J. E., and Rappold, A. G.:  
744 Wildfire and prescribed burning impacts on air quality in the United States,



- 745 <https://doi.org/10.1080/10962247.2020.1749731>, 2020.
- 746 Jaffe, D. A., Schnieder, B., and Inouye, D.: Technical note: Use of PM 2.5 to CO ratio as an indicator of wildfire  
747 smoke in urban areas, *Atmos. Chem. Phys.*, 22, 12695–12704, <https://doi.org/10.5194/acp-22-12695-2022>, 2022.
- 748 Jo, D. S., Park, R. J., Lee, S., Kim, S. W., and Zhang, X.: A global simulation of brown carbon: Implications for  
749 photochemistry and direct radiative effect, *Atmos. Chem. Phys.*, <https://doi.org/10.5194/acp-16-3413-2016>, 2016.
- 750 Kaufman, Y. J., Tucker, C. J., and Fung, I. Y.: Remote sensing of biomass burning in the tropics, *Adv. Sp. Res.*,  
751 [https://doi.org/10.1016/0273-1177\(89\)90173-7](https://doi.org/10.1016/0273-1177(89)90173-7), 1989.
- 752 Kelp, M. M., Carroll, M. C., Liu, T., Yantosca, R. M., Hockenberry, H. E., and Mickley, L. J.: Prescribed Burns as a  
753 Tool to Mitigate Future Wildfire Smoke Exposure: Lessons for States and Rural Environmental Justice  
754 Communities, *Earth's Futur.*, 11, <https://doi.org/10.1029/2022EF003468>, 2023.
- 755 Korontzi, S., Ward, D. E., Susott, R. A., Yokelson, R. J., Justice, C. O., Hobbs, P. V., Smithwick, E. A. H., and Hao,  
756 W. M.: Seasonal variation and ecosystem dependence of emission factors for selected trace gases and PM 2.5 for  
757 southern African savanna fires, *J. Geophys. Res. Atmos.*, 108, <https://doi.org/10.1029/2003JD003730>, 2003.
- 758 Kuenzer, C., Hecker, C., Zhang, J., Wessling, S., and Wagner, W.: The potential of multidiurnal MODIS thermal  
759 band data for coal fire detection, *Int. J. Remote Sens.*, <https://doi.org/10.1080/01431160701352147>, 2008.
- 760 Lack, D. A. and Langridge, J. M.: On the attribution of black and brown carbon light absorption using the Ångström  
761 exponent, *Atmos. Chem. Phys.*, 13, 10535–10543, <https://doi.org/10.5194/acp-13-10535-2013>, 2013.
- 762 Larkin, N. K., Raffuse, S. M., Huang, S. M., Pavlovic, N., Lahm, P., and Rao, V.: The Comprehensive Fire  
763 Information Reconciled Emissions (CFIRE) inventory: Wildland fire emissions developed for the 2011 and 2014  
764 U.S. National Emissions Inventory, *J. Air Waste Manag. Assoc.*, <https://doi.org/10.1080/10962247.2020.1802365>,  
765 2020.
- 766 Lee, S., Baumann, K., Schauer, J. J., Sheesley, R. J., Nacher, L. P., Meinardi, S., Blake, D. R., Edgerton, E. S.,  
767 Russell, A. G., and Clements, M.: Gaseous and Particulate Emissions from Prescribed Burning in Georgia, *Environ.*  
768 *Sci. Technol.*, 39, 9049–9056, <https://doi.org/10.1021/es051583l>, 2005.
- 769 Lee, S., Kim, H. K., Yan, B., Cobb, C. E., Hennigan, C., Nichols, S., Chamber, M., Edgerton, E. S., Jansen, J. J.,  
770 Hu, Y., Zheng, M., Weber, R. J., and Russell, A. G.: Diagnosis of Aged Prescribed Burning Plumes Impacting an  
771 Urban Area, *Environ. Sci. Technol.*, 42, 1438–1444, <https://doi.org/10.1021/es7023059>, 2008.
- 772 Levy, I., Mihele, C., Lu, G., Narayan, J., Hilker, N., and Brook, J. R.: Elucidating multipollutant exposure across a  
773 complex metropolitan area by systematic deployment of a mobile laboratory, *Atmos. Chem. Phys.*,  
774 <https://doi.org/10.5194/acp-14-7173-2014>, 2014.
- 775 Liu, D., Zhang, Q., Jiang, J., and Chen, D. R.: Performance calibration of low-cost and portable particular matter  
776 (PM) sensors, *J. Aerosol Sci.*, <https://doi.org/10.1016/j.jaerosci.2017.05.011>, 2017a.





- 777 Liu, J. C., Pereira, G., Uhl, S. A., Bravo, M. A., and Bell, M. L.: A systematic review of the physical health impacts  
778 from non-occupational exposure to wildfire smoke, *Environ. Res.*, 136, 120–132,  
779 <https://doi.org/10.1016/j.envres.2014.10.015>, 2015.
- 780 Liu, T., Marlier, M. E., Karambelas, A., Jain, M., Singh, S., Singh, M. K., Gautam, R., and Defries, R. S.: Missing  
781 emissions from post-monsoon agricultural fires in northwestern India: Regional limitations of modis burned area  
782 and active fire products, <https://doi.org/10.1088/2515-7620/ab056c>, 2019.
- 783 Liu, X., Zhang, Y., Huey, L. G., Yokelson, R. J., Wang, Y., Jimenez, J. L., Campuzano-Jost, P., Beyersdorf, A. J.,  
784 Blake, D. R., Choi, Y., St. Clair, J. M., Crouse, J. D., Day, D. A., Diskin, G. S., Fried, A., Hall, S. R., Hanisco, T.  
785 F., King, L. E., Meinardi, S., Mikoviny, T., Palm, B. B., Peischl, J., Perring, A. E., Pollack, I. B., Ryerson, T. B.,  
786 Sachse, G., Schwarz, J. P., Simpson, I. J., Tanner, D. J., Thornhill, K. L., Ullmann, K., Weber, R. J., Wennberg, P.  
787 O., Wisthaler, A., Wolfe, G. M., and Ziemba, L. D.: Agricultural fires in the southeastern U.S. during SEAC4RS:  
788 Emissions of trace gases and particles and evolution of ozone, reactive nitrogen, and organic aerosol, *J. Geophys.*  
789 *Res. Atmos.*, 121, 7383–7414, <https://doi.org/10.1002/2016JD025040>, 2016.
- 790 Liu, X., Huey, L. G., Yokelson, R. J., Selimovic, V., Simpson, I. J., Müller, M., Jimenez, J. L., Campuzano-Jost, P.,  
791 Beyersdorf, A. J., Blake, D. R., Butterfield, Z., Choi, Y., Crouse, J. D., Day, D. A., Diskin, G. S., Dubey, M. K.,  
792 Fortner, E., Hanisco, T. F., Hu, W., King, L. E., Kleinman, L., Meinardi, S., Mikoviny, T., Onasch, T. B., Palm, B.  
793 B., Peischl, J., Pollack, I. B., Ryerson, T. B., Sachse, G. W., Sedlacek, A. J., Shilling, J. E., Springston, S., St. Clair,  
794 J. M., Tanner, D. J., Teng, A. P., Wennberg, P. O., Wisthaler, A., and Wolfe, G. M.: Airborne measurements of  
795 western U.S. wildfire emissions: Comparison with prescribed burning and air quality implications, *J. Geophys. Res.*  
796 *Atmos.*, 122, 6108–6129, <https://doi.org/10.1002/2016JD026315>, 2017b.
- 797 Liu, Y., Bourgeois, A., Warner, T., Swerdlin, S., and Hacker, J.: Implementation of observation-nudging based  
798 FDDA into WRF for supporting ATEC test operations, in: In Proceedings of the WRF/MM5 Users' Workshop, 27–  
799 30, 2005.
- 800 Marsavin, A., van Gageldonk, R., Bernays, N., May, N. W., Jaffe, D. A., and Fry, J. L.: Optical properties of  
801 biomass burning aerosol during the 2021 Oregon fire season: comparison between wild and prescribed fires,  
802 *Environ. Sci. Atmos.*, 3, 608–626, <https://doi.org/10.1039/D2EA00118G>, 2023.
- 803 Martin, M. V., Kahn, R. A., and Tosca, M. G.: A global analysis of wildfire smoke injection heights derived from  
804 space-based multi-angle imaging, *Remote Sens.*, <https://doi.org/10.3390/rs10101609>, 2018.
- 805 Martinsson, B. G., Friberg, J., Sandvik, O. S., and Sporre, M. K.: Five-satellite-sensor study of the rapid decline of  
806 wildfire smoke in the stratosphere, *Atmos. Chem. Phys.*, <https://doi.org/10.5194/acp-22-3967-2022>, 2022.
- 807 May, A. A., McMeeking, G. R., Lee, T., Taylor, J. W., Craven, J. S., Burling, I., Sullivan, A. P., Akagi, S., Collett,  
808 J. L., Flynn, M., Coe, H., Urbanski, S. P., Seinfeld, J. H., Yokelson, R. J., and Kreidenweis, S. M.: Aerosol  
809 emissions from prescribed fires in the United States: A synthesis of laboratory and aircraft measurements, *J.*  
810 *Geophys. Res. Atmos.*, 119, 11,826–11,849, <https://doi.org/10.1002/2014JD021848>, 2014.





- 811 May, A. A., Lee, T., McMeeking, G. R., Akagi, S., Sullivan, A. P., Urbanski, S., Yokelson, R. J., and Kreidenweis,  
812 S. M.: Observations and analysis of organic aerosol evolution in some prescribed fire smoke plumes, *Atmos. Chem.*  
813 *Phys.*, 15, 6323–6335, <https://doi.org/10.5194/acp-15-6323-2015>, 2015.
- 814 Mildrexler, D. J., Zhao, M., Heinsch, F. A., and Running, S. W.: A new satellite-based methodology for continental-  
815 scale disturbance detection, *Ecol. Appl.*, [https://doi.org/10.1890/1051-0761\(2007\)017\[0235:ANSMFC\]2.0.CO;2](https://doi.org/10.1890/1051-0761(2007)017[0235:ANSMFC]2.0.CO;2),  
816 2007.
- 817 Naeher, L. P., Brauer, M., Lipsett, M., Zelikoff, J. T., Simpson, C. D., Koenig, J. Q., and Smith, K. R.: Woodsmoke  
818 Health Effects: A Review, *Inhal. Toxicol.*, 19, 67–106, <https://doi.org/10.1080/08958370600985875>, 2007.
- 819 Nowell, H. K., Holmes, C. D., Robertson, K., Teske, C., and Hiers, J. K.: A New Picture of Fire Extent, Variability,  
820 and Drought Interaction in Prescribed Fire Landscapes: Insights From Florida Government Records, *Geophys. Res.*  
821 *Let.*, <https://doi.org/10.1029/2018GL078679>, 2018.
- 822 O’Dell, K., Hornbrook, R. S., Permar, W., Levin, E. J. T., Garofalo, L. A., Apel, E. C., Blake, N. J., Jarnot, A.,  
823 Pothier, M. A., Farmer, D. K., Hu, L., Campos, T., Ford, B., Pierce, J. R., and Fischer, E. V.: Correction to  
824 Hazardous Air Pollutants in Fresh and Aged Western US Wildfire Smoke and Implications for Long-Term  
825 Exposure, *Environ. Sci. Technol.*, 56, 3304–3304, <https://doi.org/10.1021/acs.est.2c01008>, 2022.
- 826 Palm, B. B., Peng, Q., Fredrickson, C. D., Lee, B. H., Garofalo, L. A., Pothier, M. A., Kreidenweis, S. M., Farmer,  
827 D. K., Pokhrel, R. P., Shen, Y., Murphy, S. M., Permar, W., Hu, L., Campos, T. L., Hall, S. R., Ullmann, K., Zhang,  
828 X., Flocke, F., Fischer, E. V., and Thornton, J. A.: Quantification of organic aerosol and brown carbon evolution in  
829 fresh wildfire plumes, *Proc. Natl. Acad. Sci.*, 117, 29469–29477, <https://doi.org/10.1073/pnas.2012218117>, 2020.
- 830 Parrish, D. D., Holloway, J. S., and Fehsenfeld, F. C.: Routine, Continuous Measurement of Carbon Monoxide with  
831 Parts per Billion Precision, *Environ. Sci. Technol.*, <https://doi.org/10.1021/es00058a013>, 1994.
- 832 Pratt, K. A., Murphy, S. M., Subramanian, R., Demott, P. J., Kok, G. L., Campos, T., Rogers, D. C., Prenni, A. J.,  
833 Heymsfield, A. J., Seinfeld, J. H., and Prather, K. A.: Flight-based chemical characterization of biomass burning  
834 aerosols within two prescribed burn smoke plumes, *Atmos. Chem. Phys.*, [https://doi.org/10.5194/acp-11-12549-](https://doi.org/10.5194/acp-11-12549-2011)  
835 2011, 2011.
- 836 Prichard, S. J., O’Neill, S. M., Eagle, P., Andreu, A. G., Drye, B., Dubowy, J., Urbanski, S., and Strand, T. M.:  
837 Wildland fire emission factors in North America: synthesis of existing data, measurement needs and management  
838 applications, *Int. J. Wildl. Fire*, 29, 132, <https://doi.org/10.1071/WF19066>, 2020.
- 839 Reid, C. E., Brauer, M., Johnston, F. H., Jerrett, M., Balmes, J. R., and Elliott, C. T.: Critical Review of Health  
840 Impacts of Wildfire Smoke Exposure, *Environ. Health Perspect.*, 124, 1334–1343,  
841 <https://doi.org/10.1289/ehp.1409277>, 2016.
- 842 Saleh, R., Hennigan, C. J., McMeeking, G. R., Chuang, W. K., Robinson, E. S., Coe, H., Donahue, N. M., and  
843 Robinson, A. L.: Absorptivity of brown carbon in fresh and photo-chemically aged biomass-burning emissions,



- 844 Atmos. Chem. Phys., 13, 7683–7693, <https://doi.org/10.5194/acp-13-7683-2013>, 2013.
- 845 Schroeder, W. and Giglio, L.: NASA VIIRS Land Science Investigator Processing System (SIPS) Visible Infrared  
846 Imaging Radiometer Suite (VIIRS) 375 m & 750 m Active Fire Products: Product User’s Guide, Nasa, 1.4, 2–23,  
847 2018.
- 848 Selimovic, V., Yokelson, R. J., McMeeking, G. R., and Coefield, S.: In situ measurements of trace gases, PM, and  
849 aerosol optical properties during the 2017 NW US wildfire smoke event, Atmos. Chem. Phys., 19, 3905–3926,  
850 <https://doi.org/10.5194/acp-19-3905-2019>, 2019.
- 851 Shamarock, W. C., Klemp, J. B., Dudhia, J., Gill, D. O., Liu, Z., Berner, J., Wang, W., Powers, J. G., Duda, M. G.,  
852 Barker, D. M., and Huang, X.-Y.: A Description of the Advanced Research WRF Model Version 4,  
853 <https://doi.org/10.5065/1DFH-6P97>, 2019.
- 854 Singleton, M. P., Thode, A. E., Sánchez Meador, A. J., and Iniguez, J. M.: Increasing trends in high-severity fire in  
855 the southwestern USA from 1984 to 2015, For. Ecol. Manage., 433, 709–719,  
856 <https://doi.org/10.1016/j.foreco.2018.11.039>, 2019.
- 857 Sinha, P., Hobbs, P. V., Yokelson, R. J., Bertschi, I. T., Blake, D. R., Simpson, I. J., Gao, S., Kirchstetter, T. W., and  
858 Novakov, T.: Emissions of trace gases and particles from savanna fires in southern Africa, J. Geophys. Res. Atmos.,  
859 108, <https://doi.org/10.1029/2002JD002325>, 2003.
- 860 Stein, A. F., Draxler, R. R., Rolph, G. D., Stunder, B. J. B., Cohen, M. D., and Ngan, F.: NOAA’s HYSPLIT  
861 Atmospheric Transport and Dispersion Modeling System, Bull. Am. Meteorol. Soc., 96, 2059–2077,  
862 <https://doi.org/10.1175/BAMS-D-14-00110.1>, 2015.
- 863 Strand, T., Gullett, B., Urbanski, S., O’Neill, S., Potter, B., Aurell, J., Holder, A., Larkin, N., Moore, M., and Rorig,  
864 M.: Grassland and forest understorey biomass emissions from prescribed fires in the south-eastern United States -  
865 RxCADRE 2012, Int. J. Wildl. Fire, <https://doi.org/10.1071/WF14166>, 2016.
- 866 Sullivan, A. P., Pokhrel, R. P., Shen, Y., Murphy, S. M., Toohey, D. W., Campos, T., Lindaas, J., Fischer, E. V., and  
867 Collett Jr., J. L.: Examination of brown carbon absorption from wildfires in the western US during the WE-CAN  
868 study, Atmos. Chem. Phys., 22, 13389–13406, <https://doi.org/10.5194/acp-22-13389-2022>, 2022.
- 869 USDA: Wildfire crisis strategy implementation plan: A 10-year implementation plan, 1–11, 2022.
- 870 Virkkula, A., Ahlquist, N. C., Covert, D. S., Arnott, W. P., Sheridan, P. J., Quinn, P. K., and Coffman, D. J.:  
871 Modification, calibration and a field test of an instrument for measuring light absorption by particles, Aerosol Sci.  
872 Technol., <https://doi.org/10.1080/027868290901963>, 2005.
- 873 Virkkula, A., Mäkelä, T., Hillamo, R., Yli-Tuomi, T., Hirsikko, A., Hämeri, K., and Koponen, I. K.: A Simple  
874 Procedure for Correcting Loading Effects of Aethalometer Data, J. Air Waste Manage. Assoc., 57, 1214–1222,  
875 <https://doi.org/10.3155/1047-3289.57.10.1214>, 2007.



- 876 Wang, J., Yue, Y., Wang, Y., Ichoku, C., Ellison, L., and Zeng, J.: Mitigating Satellite-Based Fire Sampling  
877 Limitations in Deriving Biomass Burning Emission Rates: Application to WRF-Chem Model Over the Northern  
878 sub-Saharan African Region, *J. Geophys. Res. Atmos.*, <https://doi.org/10.1002/2017JD026840>, 2018.
- 879 Wise, C. R.: Accountability in Collaborative Federal Programs—Multidimensional and Multilevel Performance  
880 Measures Needed: The Case of Wildland Fire Prevention, *Am. Rev. Public Adm.*, 52, 95–108,  
881 <https://doi.org/10.1177/02750740211050367>, 2022.
- 882 Wyden, R. and Manchin, J.: National Prescribed Fire Act of 2020, , 116TH CONGRESS. 2D SESSION, 2020.
- 883 Xiu, M., Jayaratne, R., Thai, P., Christensen, B., Zing, I., Liu, X., and Morawska, L.: Evaluating the applicability of  
884 the ratio of PM<sub>2.5</sub> and carbon monoxide as source signatures, *Environ. Pollut.*, 306, 119278,  
885 <https://doi.org/10.1016/j.envpol.2022.119278>, 2022.
- 886 Yokelson, R. J., Goode, J. G., Ward, D. E., Susott, R. A., Babbitt, R. E., Wade, D. D., Bertschi, I., Griffith, D. W.  
887 T., and Hao, W. M.: Emissions of formaldehyde, acetic acid, methanol, and other trace gases from biomass fires in  
888 North Carolina measured by airborne Fourier transform infrared spectroscopy, *J. Geophys. Res. Atmos.*, 104,  
889 30109–30125, <https://doi.org/10.1029/1999JD900817>, 1999.
- 890 Yokelson, R. J., Crouse, J. D., DeCarlo, P. F., Karl, T., Urbanski, S., Atlas, E., Campos, T., Shinozuka, Y.,  
891 Kapustin, V., Clarke, A. D., Weinheimer, A., Knapp, D. J., Montzka, D. D., Holloway, J., Weibring, P., Flocke, F.,  
892 Zheng, W., Toohey, D., Wennberg, P. O., Wiedinmyer, C., Mauldin, L., Fried, A., Richter, D., Walega, J., Jimenez,  
893 J. L., Adachi, K., Buseck, P. R., Hall, S. R., and Shetter, R.: Emissions from biomass burning in the Yucatan,  
894 *Atmos. Chem. Phys.*, 9, 5785–5812, <https://doi.org/10.5194/acp-9-5785-2009>, 2009.
- 895 Yokelson, R. J., Burling, I. R., Urbanski, S. P., Atlas, E. L., Adachi, K., Buseck, P. R., Wiedinmyer, C., Akagi, S.  
896 K., Toohey, D. W., and Wold, C. E.: Trace gas and particle emissions from open biomass burning in Mexico,  
897 *Atmos. Chem. Phys.*, 11, 6787–6808, <https://doi.org/10.5194/acp-11-6787-2011>, 2011.
- 898 Yokelson, R. J., Burling, I. R., Gilman, J. B., Warneke, C., Stockwell, C. E., De Gouw, J., Akagi, S. K., Urbanski, S.  
899 P., Veres, P., Roberts, J. M., Kuster, W. C., Reardon, J., Griffith, D. W. T., Johnson, T. J., Hosseini, S., Miller, J.  
900 W., Cocker, D. R., Jung, H., and Weise, D. R.: Coupling field and laboratory measurements to estimate the emission  
901 factors of identified and unidentified trace gases for prescribed fires, *Atmos. Chem. Phys.*,  
902 <https://doi.org/10.5194/acp-13-89-2013>, 2013.
- 903 Zeng, L., Dibb, J., Scheuer, E., Katich, J. M., Schwarz, J. P., Bourgeois, I., Peischl, J., Ryerson, T., Warneke, C.,  
904 Perring, A. E., Diskin, G. S., DiGangi, J. P., Nowak, J. B., Moore, R. H., Wiggins, E. B., Pagonis, D., Guo, H.,  
905 Campuzano-Jost, P., Jimenez, J. L., Xu, L., and Weber, R. J.: Characteristics and evolution of brown carbon in  
906 western United States wildfires, *Atmos. Chem. Phys.*, 22, 8009–8036, <https://doi.org/10.5194/acp-22-8009-2022>,  
907 2022.
- 908 Zhong, M. and Jang, M.: Dynamic light absorption of biomass-burning organic carbon photochemically aged under

<https://doi.org/10.5194/egusphere-2024-1485>

Preprint. Discussion started: 4 June 2024

© Author(s) 2024. CC BY 4.0 License.



909 natural sunlight, Atmos. Chem. Phys., 14, 1517–1525, <https://doi.org/10.5194/acp-14-1517-2014>, 2014.

910

911



912 **Tables**

913 **Table 1.** The PM<sub>2.5</sub> mass, BC, and BrC NEMRs relative to CO (based on regression slopes) and correlation values  
 914 (r<sup>2</sup>) in the column to the right of each NEMR for the smoke events identified in this study\*.

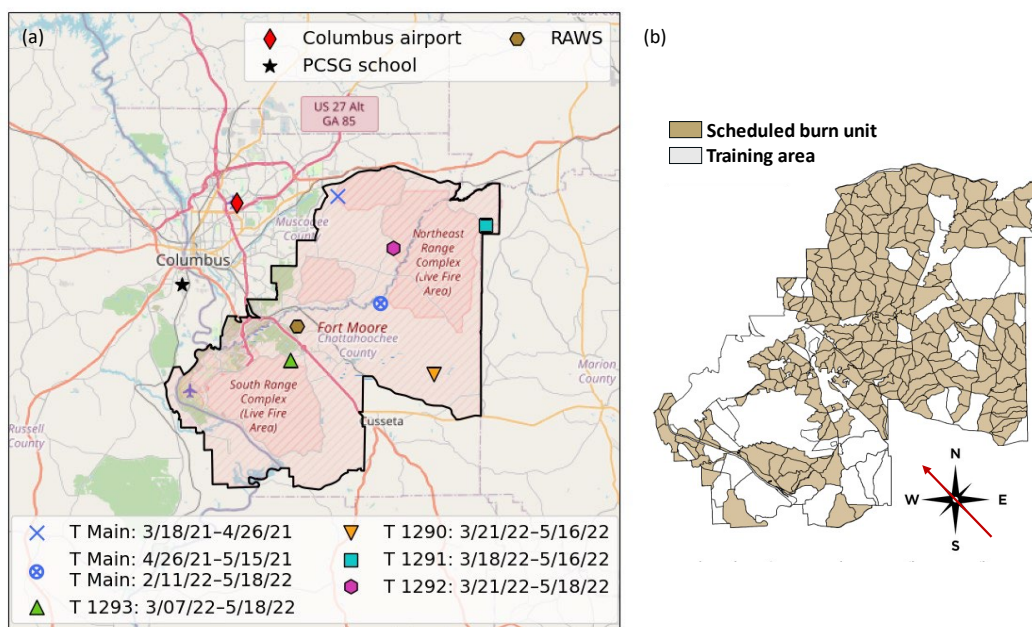
Smoke event Date/Trailer	NEMR PM <sub>2.5</sub> mass (µg m <sup>-3</sup> ppb <sup>-1</sup> )	r <sup>2</sup>	NEMR PM <sub>2.5</sub> BC (µg m <sup>-3</sup> ppb <sup>-1</sup> )	r <sup>2</sup>	NEMR PM <sub>2.5</sub> BrC (µg m <sup>-3</sup> Mm <sup>-1</sup> )	r <sup>2</sup>	Age estimated by wind vector (min)	Age estimated by HYSPLIT (min)
3/23/21 T Main	0.125	0.66	0.010	0.74	0.257	0.59	108	40
4/06/21 T Main	0.097	0.90	0.012	0.96	0.187	0.82	75	130
4/07/21 T Main	0.160	0.90	0.012	0.93	0.367	0.86	14	10
4/08/21 T Main	0.105	0.90	0.005	0.84	0.199	0.85	162	40
4/14/21 T Main	0.146	0.72	0.015	0.76	0.324	0.61	44	20
4/20/21 T Main	0.080	0.74	0.011	0.83	0.151	0.63	5	10
4/21/21 T Main	0.107	0.75	0.009	0.90	0.133	0.70	330	190
4/30/21 T Main	0.141	0.94	0.007	0.95	0.319	0.87	-	-
2/11/22 T Main	0.054	0.93	0.022	0.95	0.567	0.95	8	10
2/12/22 T Main	0.066	0.82	0.018	0.96	0.514	0.93	60	50
2/13/22 T Main	0.053	0.81	0.016	0.83	0.613	0.85	26	20
2/13/22 T Main	0.042	0.86	0.014	0.89	0.689	0.85	30	20
2/26/22 T Main	0.207	0.88	0.018	0.98	0.690	0.97	130	110
2/27/22 T Main	0.119	0.70	0.010	0.87	0.334	0.91	-	-
3/01/22 T Main	0.166	0.81	0.016	0.91	0.586	0.94	92	270
3/02/22 T Main	0.129	0.75	0.020	0.87	0.608	0.87	60	40
3/04/22 T Main	0.209	0.69	0.005	0.53	0.167	0.92	-	160
3/04/22 T Main	0.121	0.89	0.012	0.98	0.454	0.97	-	40
3/07/22 T Main	0.122	0.82	0.009	0.96	0.405	0.96	224	-
3/07/22 T Main	0.170	0.66	0.012	0.97	0.338	0.89	-	10
3/14/22 T Main	0.138	0.82	0.010	0.93	0.575	0.88	-	20
3/25/22 T Main	0.090	0.78	0.009	0.86	0.375	0.91	5	10
3/29/22 T Main	0.121	0.68	0.008	0.68	0.420	0.76	5	10
4/04/22 T Main	0.129	0.90	0.009	0.96	0.551	0.92	168	130
4/25/22 T Main	0.283	0.83	0.022	0.91	1.382	0.77	169	90
5/09/22 T Main	0.237	0.96	0.008	0.94	0.324	0.94	330	150
3/21/22 T 1293	0.188	0.98	-	-	-	-	89	20
3/25/22 T 1293	0.158	0.93	-	-	-	-	45	30
3/26/22 T 1293	0.148	0.97	-	-	-	-	5	10
3/27/22 T 1293	0.176	0.84	-	-	-	-	5	10
3/28/22 T 1293	0.129	0.81	-	-	-	-	-	60
3/29/22 T 1293	0.093	0.87	-	-	-	-	-	210
4/05/22 T 1293	0.277	0.91	0.016	0.78	0.280	0.47	-	360
4/21/22 T 1293	0.466	0.98	0.024	0.83	1.55	0.48	78	-
4/23/22 T 1293	0.121	0.59	0.013	0.80	0.317	0.33	28	10
4/23/22 T 1293	0.165	0.97	0.014	0.96	0.354	0.94	48	10
4/24/22 T 1293	0.248	0.90	-	-	-	-	63	40
4/26/22 T 1293	0.182	0.96	-	-	-	-	106	-
5/09/22 T 1293	0.238	0.99	0.012	0.98	0.321	0.94	480	210
5/10/22 T 1293	0.112	0.92	0.008	0.83	0.406	0.78	474	160
5/11/22 T 1293	0.168	0.77	-	-	-	-	5	10
5/12/22 T 1293	0.119	0.94	-	-	-	-	5	10
5/09/22 T 1291	0.265	0.98	-	-	-	-	296	160

915 \* The table lists all events where both PM<sub>2.5</sub> mass and CO concentration were both available. In some cases BC and  
 916 BrC data was not available and left as blank values (-).

917



918 **Figures**



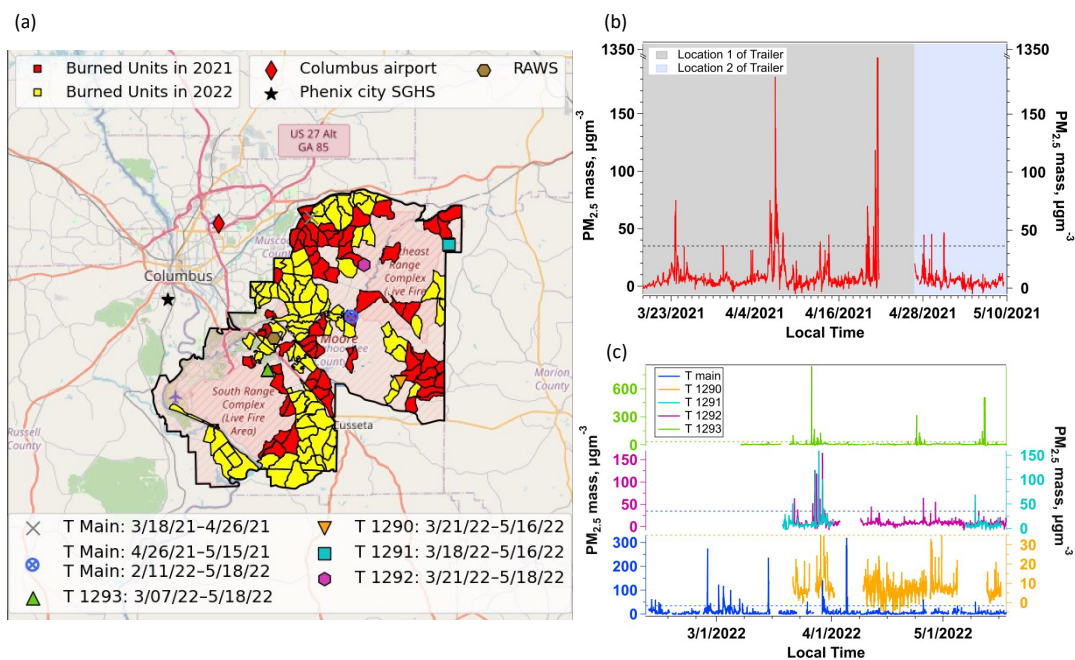
919

920 **Figure 1.** Study region overview. (a) Fort Moore map with the locations of trailers, RAWs weather station, and two  
921 state-operated sampling sites, Columbus Airport and Phenix City South Girard (PCSG) school, are shown along  
922 with the location of the city of Columbus GA. (b) Fort Moore map showing the planned burn units for the year 2021,  
923 sourced from Fort Moore authorities and natural resources management team, with prevailing winds in the region.

924



925



926

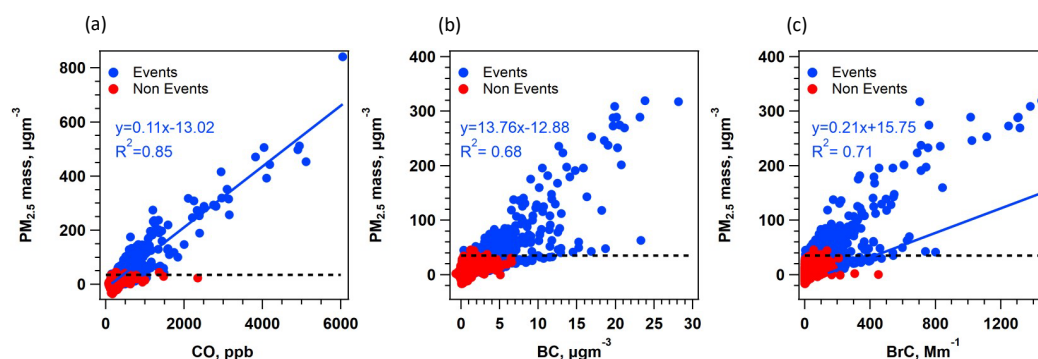
927 **Figure 2.** PM<sub>2.5</sub> mass measurements over two years study of burning. (a) Map of the burnt areas in the years 2021  
 928 and 2022 and locations of monitoring sites (b) Time series of 20-minutes average PM<sub>2.5</sub> mass concentration  
 929 measured at the main trailer during the burning season of 2021, and (c) 2022 across different sites. Dotted lines  
 930 represent PM<sub>2.5</sub> mass concentration of 35 µg m<sup>-3</sup> above which peaks were selected for detailed analysis.

931





932



933

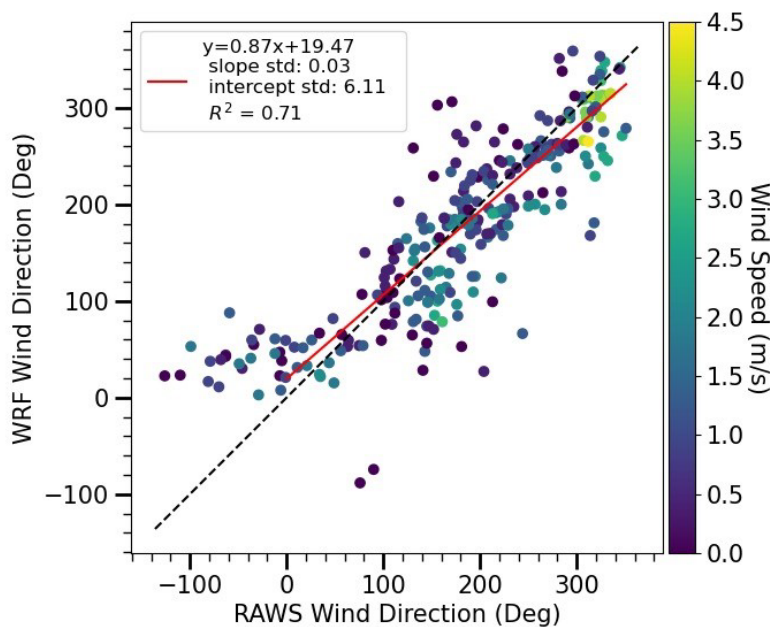
934 **Figure 3.** Correlations between PM<sub>2.5</sub> mass concentration and CO, PM<sub>2.5</sub> BC and PM<sub>2.5</sub> BrC for measurements from  
935 the main trailer in 2021 and 2022 and T1291 and T1293 in 2022. Blue data points are characterized as PM<sub>2.5</sub> events  
936 when the concentration is  $> 35 \mu\text{g m}^{-3}$  averaged over a 20-minute period. In the plot all data associated with an  
937 identified event is shown as blue (This includes event data down to the background levels before and after the peak).  
938 All other data (non-events) are shown in red. Slope is from orthogonal distance regression (ODR) of the 20-minute  
939 averaged data during events periods.

940





941



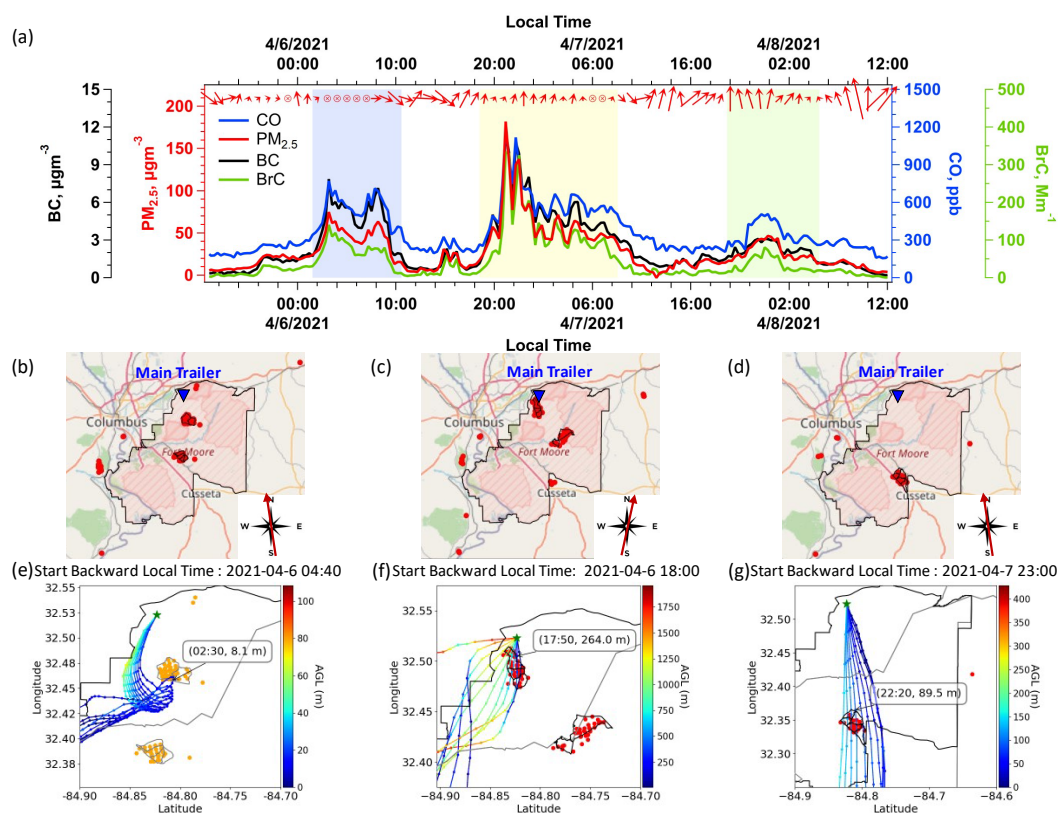
942

943 **Figure 4.** Comparison between wind direction modeled via WRF versus that recorded by the RAWS located on Fort  
944 Moore. Slope is from orthogonal distance regression (ODR).

945



946



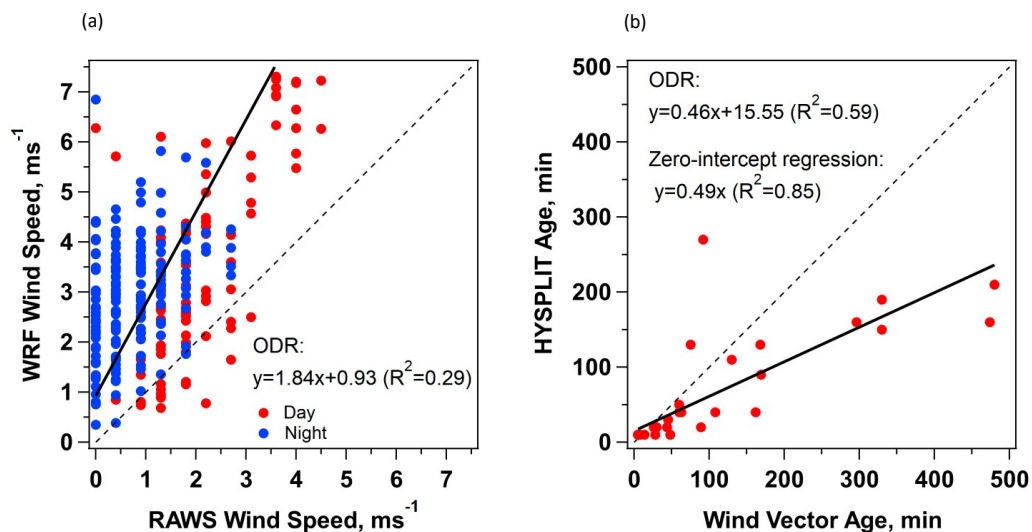
947

948 **Figure 5.** Three case studies illustrating the application of our method in determining the source of smoke events.  
 949 (a) Timeseries of species measured on main trailer. Time resolution is 20 minutes for CO, PM<sub>2.5</sub> mass, BC, and BrC.  
 950 The wind vectors depict hourly data obtained from RAWS, with the direction of the arrow indicating wind direction,  
 951 while the length of the arrow represents wind speed. (b,c,d) maps of the Fort showing historical satellite data from  
 952 the FIRMS website observed for April 5, 6, and 7, 2022. Red dots represent fires detected by the satellite. (e,f,g) are  
 953 HYSPLIT back trajectories during the occurrence of each of the three peaks. Date and time of the backward  
 954 trajectory is indicated on top of each map. Time and height at which the trajectory crosses the trailer is shown in the  
 955 box inside each map. Red dots are fires detected on FIRMS the same day of the backward trajectory. Orange dots  
 956 are fires detected on FIRMS one day before the day of the backward trajectory. The colors of the scatter are the  
 957 height above ground level. Green star marks the location of the main trailer. Satellite overpasses times are shown in  
 958 Table S8.

959



960



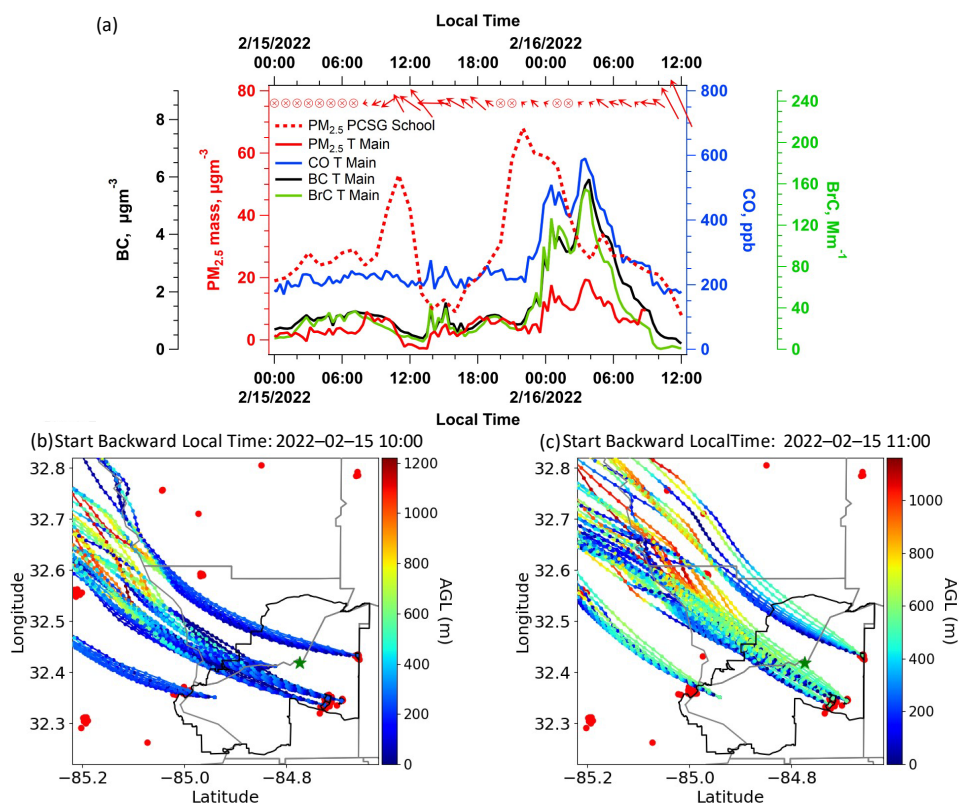
961

962 **Figure 6.** (a) Comparison between wind speed modeled via WRF versus that observed by RAWS located on Fort  
963 Moore. (b) Comparison between age estimated using HYSPLIT model vs wind vector method.

964



965



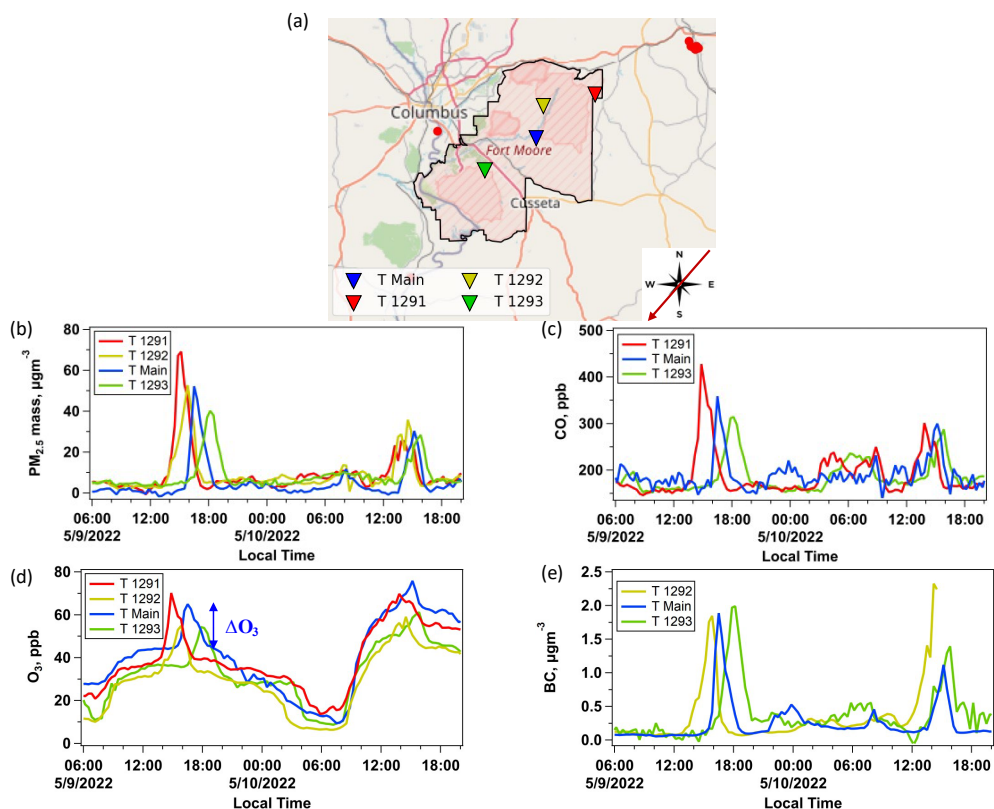
966

967 **Figure 7.** Case study of missing smoke at monitoring site despite expectations according to wind direction. (a) Time  
 968 series of species measured on main trailer. Time resolution is 20 minutes for CO, PM<sub>2.5</sub> mass, BC, and BrC. The  
 969 wind vectors depict hourly data sourced from RAWS, with the direction of the arrow indicating wind direction,  
 970 while the length of the arrow represents wind speed. Data from PCSG school are hourly averages; (b, c) HYSPLIT  
 971 forward trajectories starting from the two prescribed fires on the base on February 15, 2022 at 10:00 and 11:00,  
 972 respectively. Red dots are fires detected on FIRMS the same day (satellite overpass happened on February 15, 2022  
 973 at 12:54, 13:49, 14:32, and 14:36).

974



975



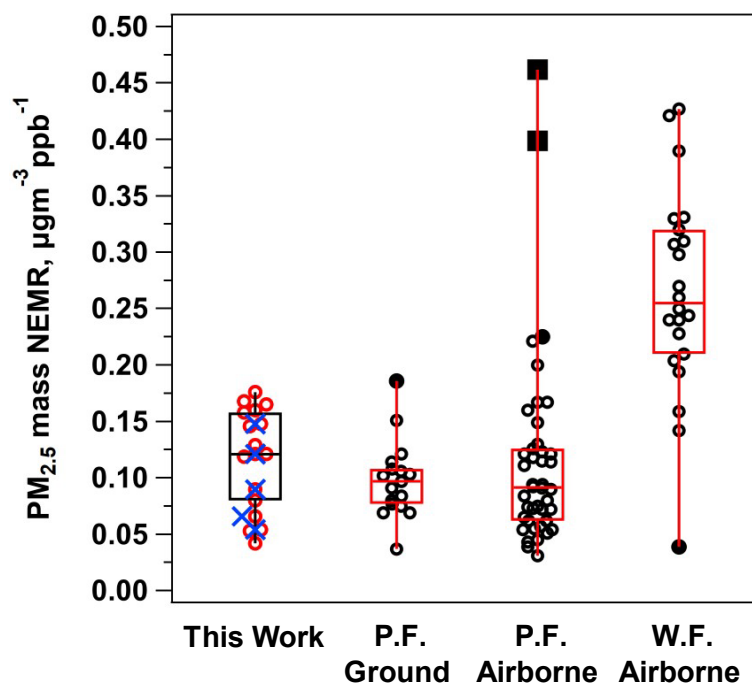
976

977 **Figure 8.** Case study of smoke detection sequentially on 4 monitoring trailers. (a) Map of the Fort showing  
 978 historical satellite data from the FIRMS website observed for May 9, 2022 (satellite overpass happened on May 9,  
 979 2022 at 12:38, 13:54, and 14:42) and average wind vector from 13:00 to 16:00 local time. Time series showing 20  
 980 minutes data of (b) PM<sub>2.5</sub> mass and (c) CO on main trailer, (d) O<sub>3</sub> concentration, and (e) BC concentration for, main  
 981 trailer, T1291, T1292, and T1293. Note that no CO instrument was operating on T1292 and no BC data for T1291.

982



983



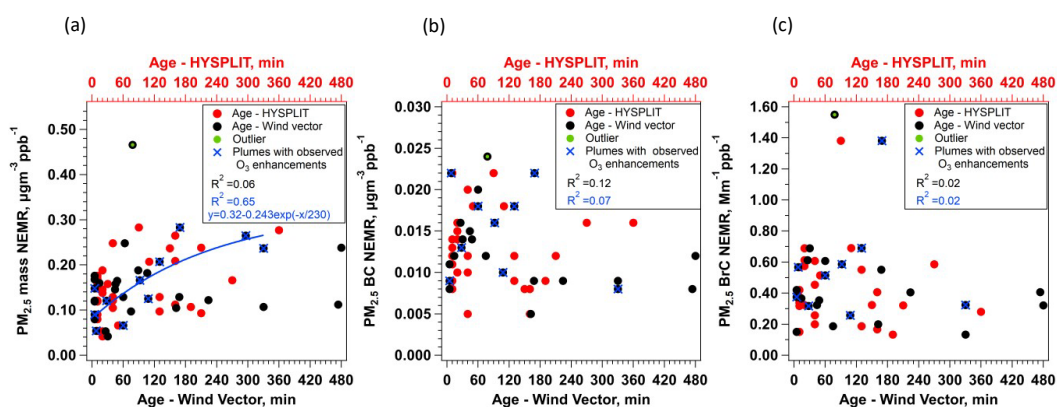
984

985 **Figure 9.** Box plot of  $PM_{2.5}$  mass NEMRs of smoke events of estimated age  $\leq 1$  hour in this study in comparison to  
986 other studies. Blue symbols in This Work are smoke plumes with observed  $O_3$  enhancements. The horizontal line  
987 inside the box represents the median of the data. The top line of the box represents the third quartile (Q3), and the  
988 bottom line represents the first quartile (Q1). Colored circles and squares represent data outliers and far outliers  
989 respectively. P.F. is Prescribed Fires, W.F. is wildfires. Some of the emission ratios reported in literature and  
990 included in the plot corresponds to  $\Delta OA/\Delta CO$  since OA tends to dominate  $\Delta PM_{2.5}$  mass concentration. (see Table  
991 S10).

992



993



994

995 **Figure 10.** (a) PM<sub>2.5</sub> mass, (b) BC, and (c) BrC NEMRs of all studied smoke events as a function of age estimated

996 using average wind vector and HYSPLIT analysis. Smoke plumes with observed O<sub>3</sub> enhancements are identified.

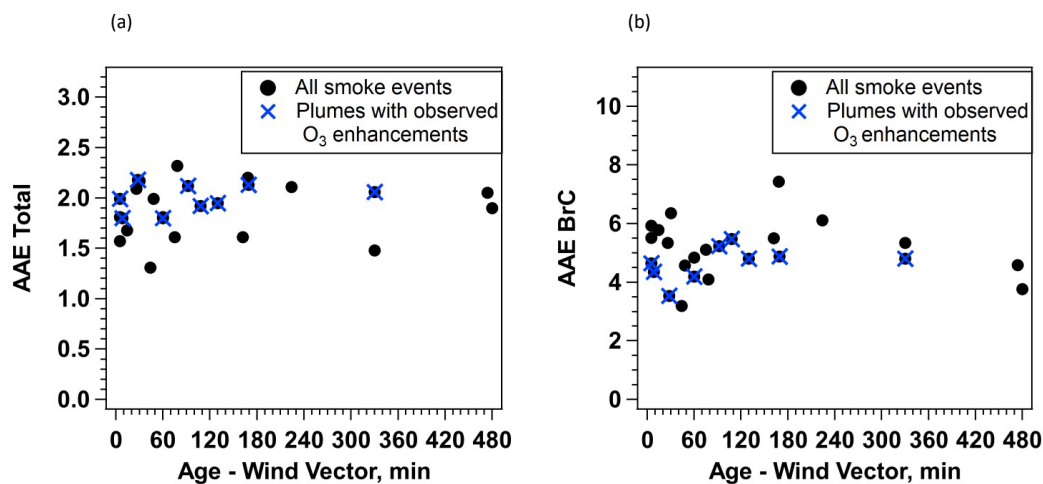
997 Linear regression coefficients of variation ( $r^2$ ) for all data and for just O<sub>3</sub> enhancement periods are identified.

998 Exponential fit equation for PM<sub>2.5</sub> mass NEMRs for O<sub>3</sub> enhancement periods is shown in (a).

999



1000



1001

1002 **Figure 11.** Average AAE values for a) total (BC+BrC) and b) BrC species for all smoke events of which  
1003 aethalometer data is available. Smoke plumes with observed O<sub>3</sub> enhancements are identified.

1004

1005

1006

1007

1008

1009